Spring 2020

Gel Permeation Chromatography Purification and Surface Chemistry of Technologically Relevant Colloidal Quantum Dots

Adam Roberge

GEL PERMEATION CHROMATOGRAPHY PURIFICATION AND SURFACE CHEMISTRY OF TECHNOLOGICALLY RELEVANT COLLOIDAL QUANTUM DOTS

by

Adam Roberge

Bachelor of Science
Waynesburg University, 2013

Submitted in Partial Fulfillment of the Requirements

For the Degree of Doctor of Philosophy in

Chemistry

College of Arts and Sciences

University of South Carolina

2020

Accepted by:

Andrew B. Greytak, Major Professor

Thomas Vogt, Committee Member

Morgan Stefik, Committee Member

Krishna Mandal, Committee Member

Cheryl L. Addy, Vice Provost and Dean of the Graduate School

Dedication

This dissertation is dedicated to **my wife Kaleigh,** whose unwavering support made all of this possible; **my son Derek,** whose smile and adoration brightened even the darkest of days; **my parents Rob & Tina,** for never doubting me even when I didn't believe in myself and always speaking words of encouragement to me; **my in-laws Jim Keri,** for providing needed reprieve from the stresses of graduate school and parenthood. Without support from each and every one of you, this would not have been possible.

Acknowledgements

I would like to gratefully thank Dr. Greytak for endless guidance and encouragement. The entire Greytak lab past and present for experimental help and experimental insight. Committee members: Dr. Thomas Vogt, Dr. Morgan Stefik, Dr. Krishna Mandal. Dr. Perry Pellechia for help with NMR spectroscopy and analysis. I would also like to thank Dr. Yi Shen for training me and providing me with many useful tips and tricks to help in experimental design and execution. Dr. Megan Gee for always taking the time to ensure proper caffeination and providing research feedback.

Abstract

Semiconductor quantum dots have received extensive research interest due to the size tunable band gap, large extinction coefficient, and ease of synthesis. These nanocrystals possess large surface to volume ratios and the chemistry at the surface of the nanocrystal greatly influences the resultant optoelectronic properties. Therefore, after synthesis, purification of the quantum dot samples to remove synthetic by-products that may alter these properties is of great importance. Gel permeation chromatography (GPC), a form of size exclusion chromatography, has been shown to reproducibly purify CdSe quantum dots. This work focuses on the expansion of purification by gel permeation chromatography to other quantum dot systems. Furthermore, utilizing the subtle purification available through gel permeation chromatography the surface chemistry of III-V and IV-VI quantum dots is investigated.

Table of Contents

List of Tables

List of Figures

CHAPTER 1

Introduction

1.1 Introduction to quantum dots

The term quantum dot refers to a semiconductor nanocrystal that has all three spatial dimensions on the order of or smaller than the Bohr exciton radius and as a result exhibits quantum confinement. The nanocrystals exhibit size tunable band gaps that afford the opportunity to span a spectroscopic range by merely altering the nanocrystal dimensions. Quantum dots have large extinction coefficients and narrow emission linewidths, making them suitable candidates for a wide array of optical applications.[1]

Quantum dots are often described as an inorganic nanocrystal core with ligands providing surface dangling bond termination. It has been shown that these ligands play a large role in the resultant optoelectronic properties of the quantum dot sample.[2,3] Therefore, it is important to pay careful attention to the binding of these ligands to the quantum dots as well as any subsequent treatments that may perturb their environment. The classification of these ligands at the surface has taken on the language used in Green's covalent bond classification.[4,5] The types of ligand (Figure 1.1) are classified by the nature of the electronic contribution the quantum dot.

1.2 Quantum dot synthetic techniques

Since the seminal paper of Murray et al in 1993[6], there has been extensive research devoted to improving quantum dot synthesis not only in synthetic yield but also in monodispersity of the product. Their initial reaction used pyrophoric and often difficult

to work with reagents such as dimethylcadmium and bistrimethylsilyl sulfide. This reaction is colloquially known as “hot injection” synthesis where the second precursor is rapidly injected to the first precursor at elevated temperature. This leads to rapid nucleation of the QDs followed by a period of growth. The reaction is quenched to halt the growth process at the desired nanocrystal size.

Hot injection has been used to create wide array of QDs with varying compositions. This technique typically provides excellent control of the QD size distribution, however, in some cases quenching the reaction at the desired QD size is difficult resulting in particles larger or smaller than desired. Furthermore, this method has seen difficulty in scale up as the reaction relies on rapid mixing of the two precursors and then subsequent quenching of the solution. Both of which present issues when scaling up for mass production.[7]

One method that was developed to circumvent the issues of hot injection is what is known as the heat up method. In this synthetic method the reactants are combined at low temperature and the temperature is then elevated to the desired growth temperature (Figure 1.2). As the temperature is increased the precursors react to form monomers and with further temperature increase reach a point of supersaturation that leads to nucleation and subsequent growth.

This method has been shown to provide better scalability compared to hot injection however, it has been more difficult to adapt to as wide an array of QD compositions as has been accessible through hot injection. One of the challenges associated with the heat up method is precursor selection as both precursors need to be soluble in the growth solvent at room temperature.

1.3 Quantum dot purification techniques

Some of the most successful synthetic techniques that have good yield and size distribution result, often have excess ligands, unreacted precursor, and synthetic byproducts remaining in solution with the nanocrystals. These often negatively impact performance of the quantum dots. Therefore, purification to remove these byproducts is required. There have been multiple methods developed to isolate quantum dots from the synthetic reaction mixture.

The most common of these methods is known as precipitation and redissolution. This method takes advantage of an anti-solvent to flocculate the particles increasing their sedimentation velocity. Then through the use of centrifugation, the particles are separated from the synthetic mixture and dispersed in neat solvent. Frequently, the quantum dots and impurities have similar solubilities and are not separated from the nanocrystal and therefore requires multiple cycles of precipitation and redissolution to remove the majority of the synthetic impurities. Furthermore, this method requires removal of solvent leaving a dried quantum dot pellet, which can cause irreversible aggregation of the particles degrading their optical properties.

Quantum dots have also been purified using extraction, which is thought to be a gentler process as the quantum dots remain in solution throughout the purification. By taking advantage of differences in solubility of the ligand stabilized quantum dots and synthetic impurities the quantum dots can be purified. This method however often requires multiple cycles to the finite differences in the solubility differences between the quantum dots and the impurities.[8]

1.4 Quantum dot characterization

Since quantum dots have size tunable band gaps one important parameter to determine in a sample is the inorganic nanocrystal size. This can be achieved through electron microscopy, dynamic light scattering, as well as small angle x-ray scattering to name a few. Many common quantum dot samples contain transition metals or other elements with a large contrast in electron of x-ray scattering increasing the resolution in the measurements.

Synthetic methods that afford good control of the quantum dot size and size distribution often yield colloidal quantum dots with the inorganic nanocrystal core passivated with organic ligands that not only provide colloidal stability but also terminate the dangling bonds of the undercoordinated crystal facets. These organic ligands have been found to greatly influence the optoelectronic properties of the quantum dot; therefore, it is paramount to be able to characterize these ligands for not only identity but also coordination and quantity. Nuclear magnetic resonance spectroscopy has been is a common method used for ligand identification as well as quantification.[9] Ligands that are bound the nanocrystal often experience a slower rotational diffusion compared to ligands that are free in solution and this has the effect of broadening the NMR signal. This difference in line shape has been used to differentiate ligands that are bound to the surface of the nanocrystal from those that are weakly associated or free in solution. Furthermore, with the use of an internal standard it is possible to determine a concentration of ligands in the quantum dots sample.

1.5 Figures

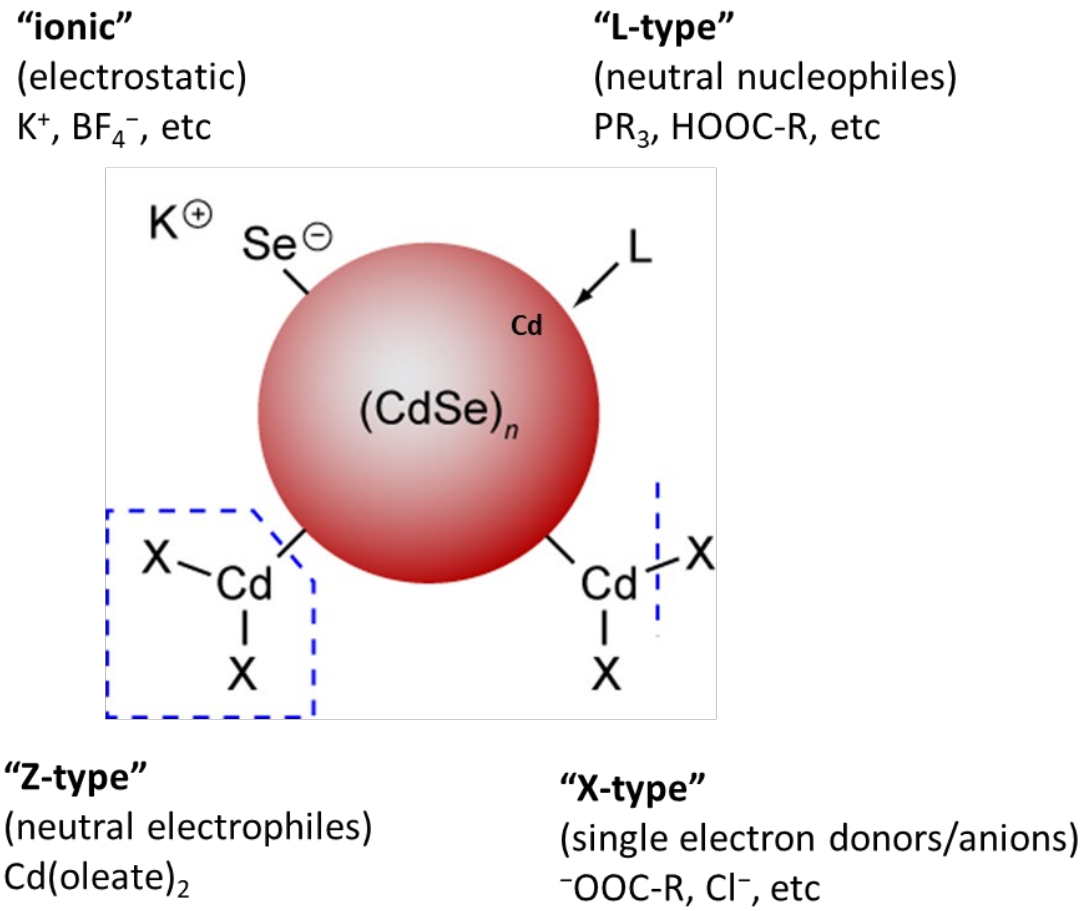

Figure 1.1 Ligand classifications for representative quantum dot sample (CdSe)

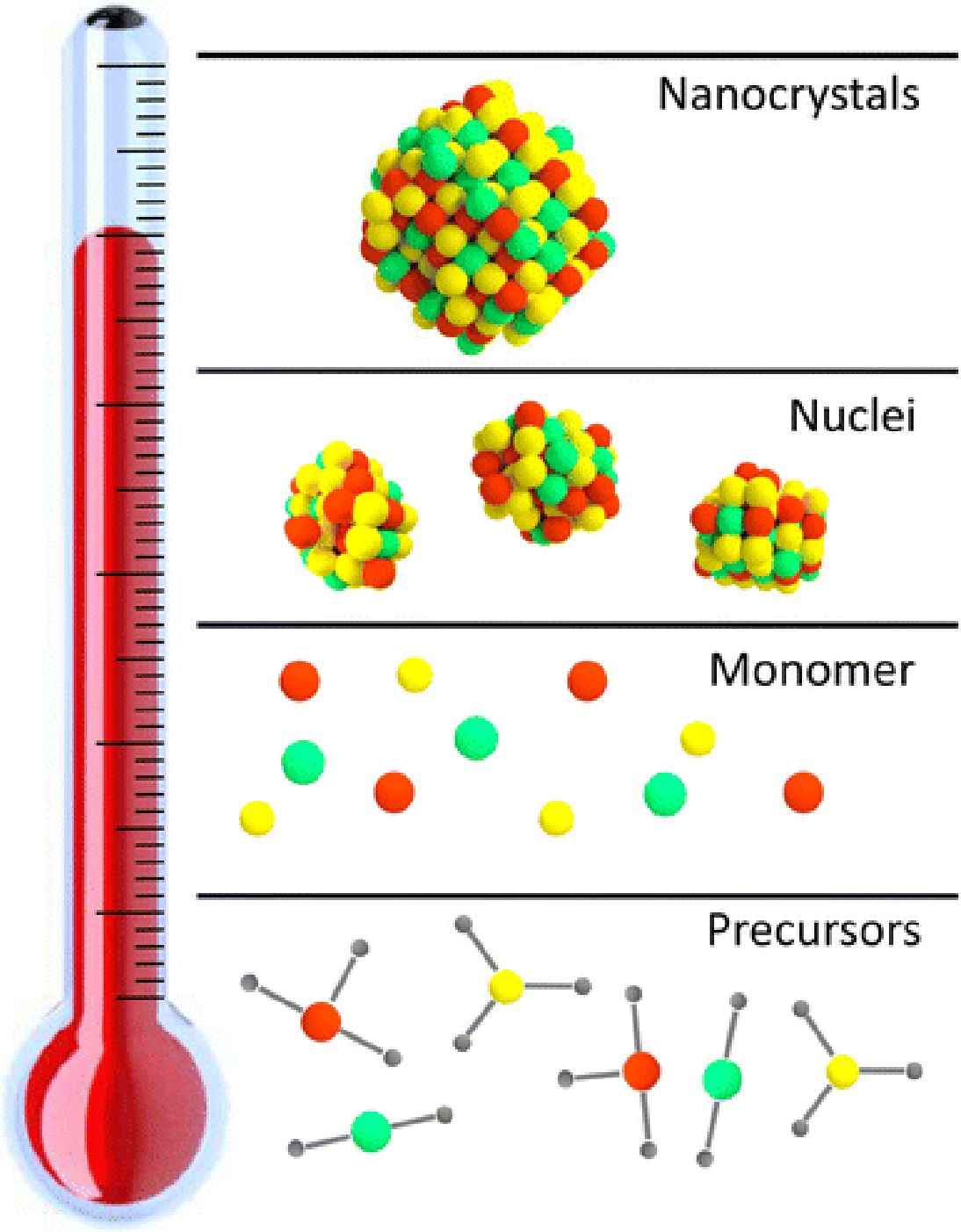

Figure 1.2 “Heat-up” synthetic method

Chapter 2

Gel Permeation Chromatography Purification of III-V Quantum Dots

2.1 Purification of air sensitive samples

Gel permeation chromatography has been demonstrated as an efficient way to purify quantum dots, namely CdSe quantum dots. Here we work to show the expansion of GPC purification to III-V quantum dots such as InP. III-V QDs are attractive samples for optoelectronic applications because of the range of visible and near infrared wavelengths accessible.[10] Furthermore, there is a desire to move away from the more toxic cadmium and lead based systems. InP QDs however rapidly oxidize in air causing irreversible etching to nanocrystal core and subsequently altering the photoluminescent properties.[11] To circumvent this issue, it is advantageous to perform GPC in an inert atmosphere. As can be seen in Figure 2.1, we packed a GPC column inside our nitrogen atmosphere glovebox. After rinsing the column with neat toluene to eliminate free polystyrene in the eluent, a sample of InP QDs in toluene was purified on the column (Figure 2.1). The sample eluted with minimal band broadening and was collected within 2 mL of eluent. UV-Vis absorption spectra (Figure 2.2) show minimal change after GPC purification to the 1s peak indicating that the nanocrystal core wasn't etched by GPC purification.

To further investigate the InP nanocrystals scanning transmission electron microscopy was to image the nanocrystals. The particles can be clearly observed by

transmission electron microscopy (Figure 2.3). The weaker Z-contrast of InP to the support film means that frequently an electron shower is often required to reduce the impact of organic ligands on the recorded images. However, after GPC purification high quality InP images could be recorded with significantly shorter beam shower times or without this treatment entirely indicating that a large portion of the organic species in the sample were removed by purification. Thermogravimetric analysis can also be used to investigate this change (Figure 2.4). The smaller mass loss after GPC purification shows that the purification removed organic matter from the samples. ^{1}HNMR of the InP sample (Figure 2.5) shows a reduction in the oleyl containing species associated with the synthetic byproducts.

2.2 InP extinction coefficient

Purification of InP QDs by GPC allows us to eliminate unbound or weakly-associated small molecule species. Chemical analysis of purified samples via ICP-MS (Table 2.1) and ^{1}H NMR (Table 2.2 and Figure 2.6) enable determination of the empirical formula. When combined with high-resolution STEM (Table 2.3 and Figure 2.7) image analysis to determine particle size, an estimate of the characteristic chemical formula for one particle and the molar extinction coefficient can be obtained. We define a number of moles nQ that, when brought to a volume of 1 mL and measured on a path length of 1 cm, leads to an absorbance of 1 AU at a reference wavelength (here 350 nm). This is convenient because the number of moles in any particular sample of the same QDs can be related to nQ based on the actual absorbance and volume: $n= (V/(1\ mL))*A_{350}*nQ$. The value of nQ is related to the molar extinction coefficient by: $nQ = (10^{-3}\ L)/\epsilon_{350}$.

We assume the purified QDs can be described by an empirical chemical formula $(InP)_{a-b}(InL_3)_b$, where a and b represent the coefficients for total In and surface In respectively, and L represents a carboxylate ligand. Through chemical analysis, we can obtain the number of moles of indium nIn (Table 2.1), of ligand nL (Table 2.2), and potentially of phosphorus nP, contained in a sample of known volume V and absorbance A_{350}. Then, coefficients a and b can be obtained, but for a factor nQ, as:

$$a\ nQ = \frac{nIn}{A_{350} \times V/1\ mL}$$

$$b\ nQ = \frac{nL/3}{A_{350} \times V/1\ mL}$$

These values have units of moles and the ratio of "surface" (ligand-balanced) to "bulk" (phosphide-balanced) In, given by b/(a-b), can be obtained and was found to have a value of 0.78. STEM imaging (Table 2.3 and Figure 2.7) of many QDs allows the average volume of a QD to be estimated from the distribution of projected areas. This volume V_{QD} can be compared to the molar volume of solid InP to find nQ based on the numbers from the empirical formula, in two ways. Method 1: The STEM mapping is most sensitive to In atoms, so one approach is to simply use V_{QD}/V_m to find the amount of indium. The molar volume V_m is ¼ of the cubic zincblende unit cell volume for InP. Thus:

$$a = \frac{V_{QD}}{V_m}$$

$$\left(\frac{1}{nQ}\right) a\ nQ = \frac{V_{QD}}{V_m}$$

so

$$\left(\frac{1}{nQ}\right) = \frac{V_{QD}/V_m}{a\ nQ}$$

$$nQ= \frac{a\ nQ}{V_{QD}/V_m}$$

Substituting a nQ from the chemical analysis above gives nQ, and b. Method 2: The QD is not pure InP, but we consider the STEM size to reflect the total number of In and P atoms:

$$2(a-b)+b=\frac{V_{QD}}{V_m/2}$$

Where $V_m/2$ represents the volume per atom in the solid (2 per formula unit of InP). This can be re-written as:

$$\left(\frac{1}{nQ}\right)(2a\ nQ-b\ nQ)=2\frac{V_{QD}}{V_m}$$

so

$$\left(\frac{1}{nQ}\right)=2\frac{(V_{QD}/V_m)}{(2a\ nQ-b\ nQ)}$$

$$nQ=\left(\frac{2a\ nQ-b\ nQ}{2\ V_{QD}/V_m}\right)$$

Once nQ is found (by substituting a nQ and b nQ from the chemical analysis), values for a and b can be obtained. The overall effect, when compared to the first method above, is a somewhat smaller value for nQ, noting that in the presence of substantial surface indium content method 1 may underestimate the amount of material per QD. Calculation using method 1 yields a value of $nQ = 8.43 \times 10^{-10}$ corresponding to an extinction coefficient $\varepsilon_{350} = 1.19 \times 10^6$ L/(mol×cm). Method 2 yields $nQ = 6.58 \times 10^{-10}$ corresponding to an extinction coefficient $\varepsilon_{350} = 1.52 \times 10^6$ L/(mol×cm). Using the ratio of "surface" (ligand-balanced) to "bulk" (phosphide-balanced) In calculated above (0.78) a chemical formula of the InP particles is calculated to be $In_{525}P_{294}$. These experiments provide evidence that gel permeation chromatography can be utilized in an inert

environment to successfully purify air sensitive samples expanding the scope of materials that can be purified by gel permeation chromatography.

2.3 Tables and figures

Table 2.1 ICP-MS of InP quantum dots to determine total In content

ppb	Sample (g)	[In] (mg/kg)	L sample	Sample (kg)	g In	mol In	
3.83E+04	8.90E-03	2.84E+05	2.00E-04	8.90E-06	2.53E-03	2.20E-05	
4.42E+04	1.24E-02	2.63E+05	2.50E-04	1.24E-05	3.26E-03	2.84E-05	
4.19E+04	1.27E-02	2.76E+05	2.50E-04	1.27E-05	3.50E-03	3.05E-05	**a nQ**
					nIn	**8.09E-05**	**3.45E-07**

Table 2.2 Calculation of moles of surface In based on ^{1}H NMR integrations from Figure 2.6

Peak Integral		Peak Integral					
CH_3	[MA]	CH_2	[MA]	average [MA]	nL	**nL/3**	**b nQ**
2.12E+02	1.06E-01	1.70E+03	1.07E-01	1.07E-01	1.07E-04	**3.55E-05**	**1.51E-07**

Table 2.3. Calculation of total atoms per quantum dots using size from STEM (Figure 2.7)

Radius (nm)	V_{QD} (nm^3)	a	unit cell v (nm^3)	V_m	**2 (V_{QD}/V_{m})**
1.68	20.7	0.587	0.202	0.0505	**819**

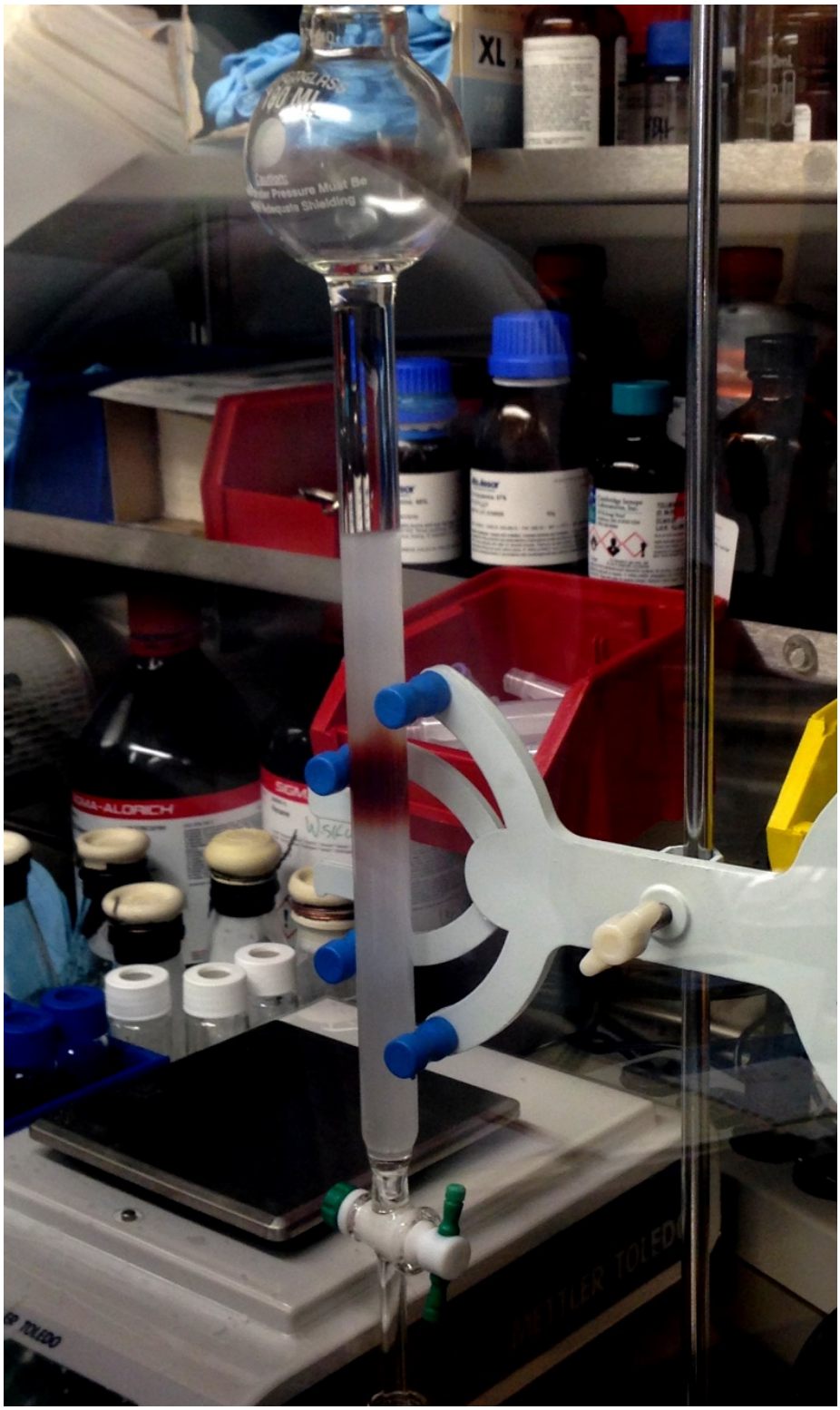

Figure 2.1 InP QD sample on a GPC column in a nitrogen glovebox

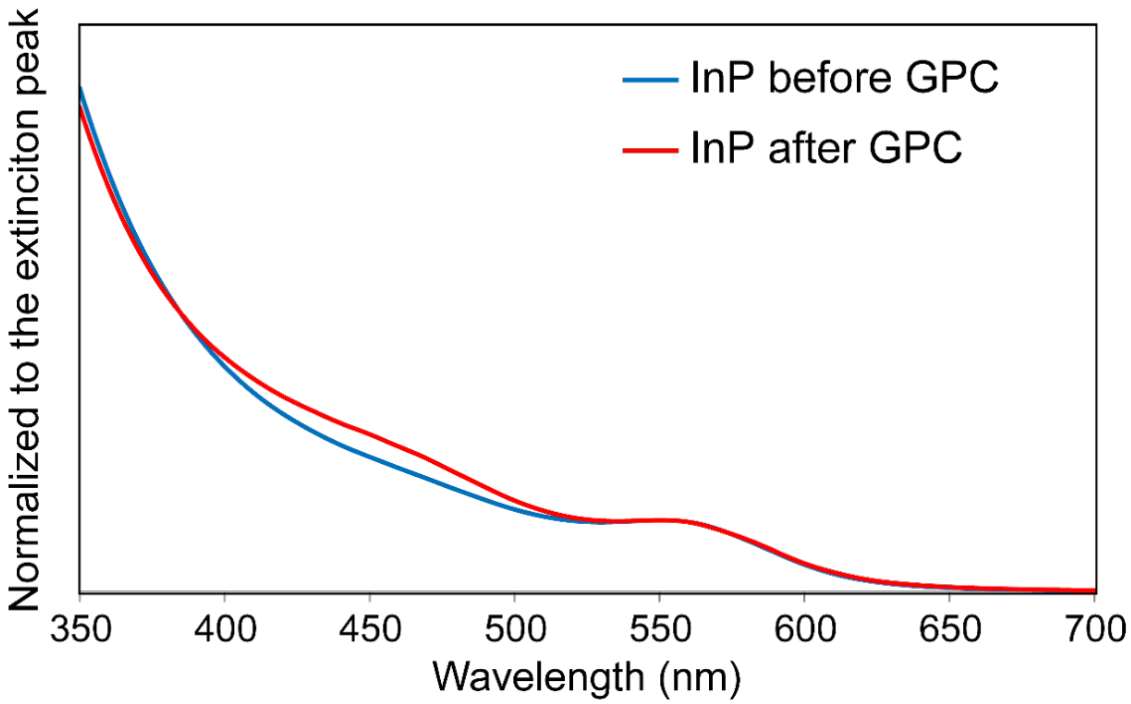

Figure 2.2 InP QD absorbance spectra before and after GPC purification

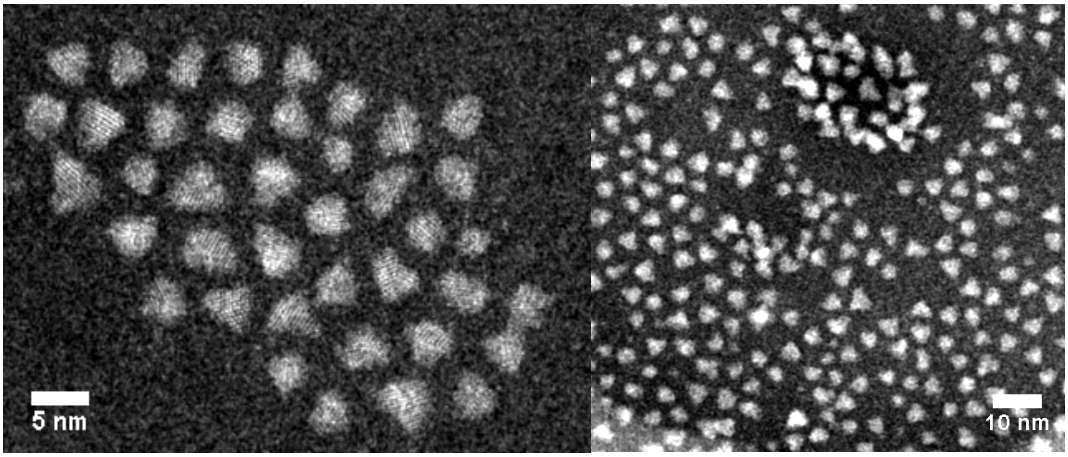

Figure 2.3 Scanning transmission electron microscopy image of InP samples

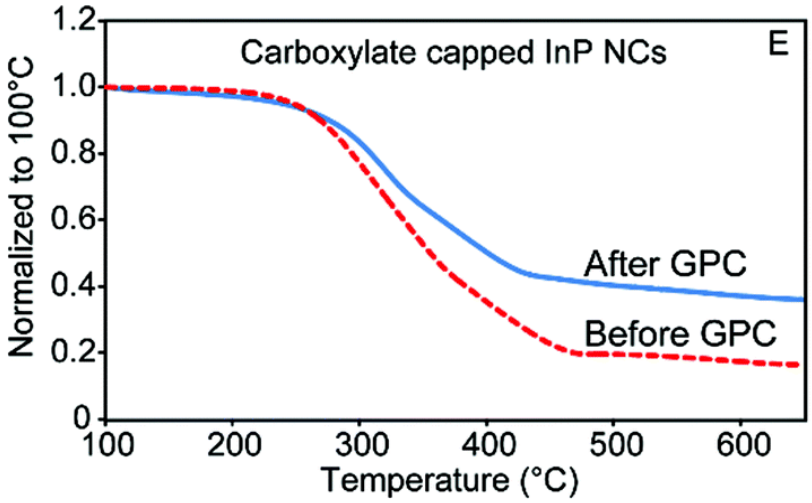

Figure 2.4 Thermogravimetric analysis of InP before and after GPC purification

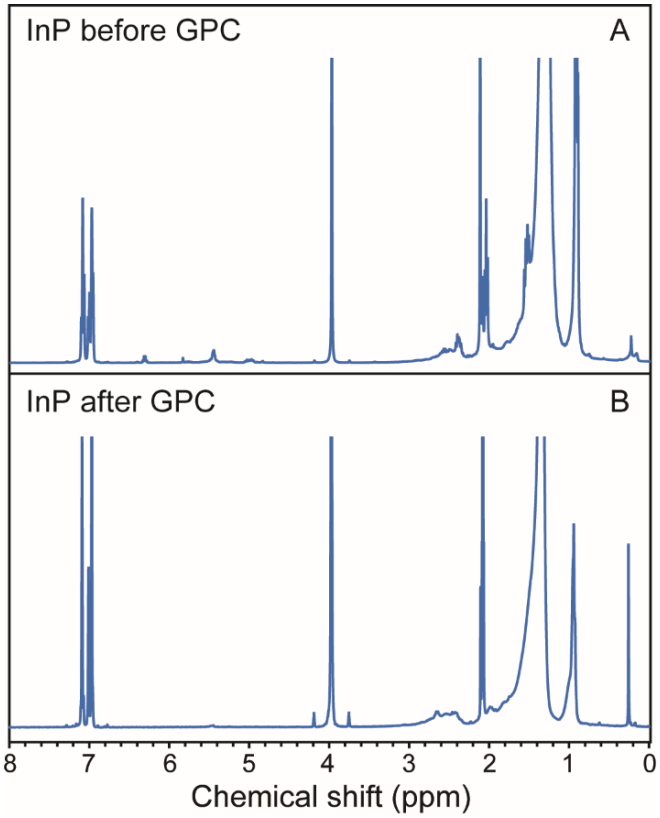

Figure 2.5 HNMR spectra of InP QDs showing reduction of olefin containing species

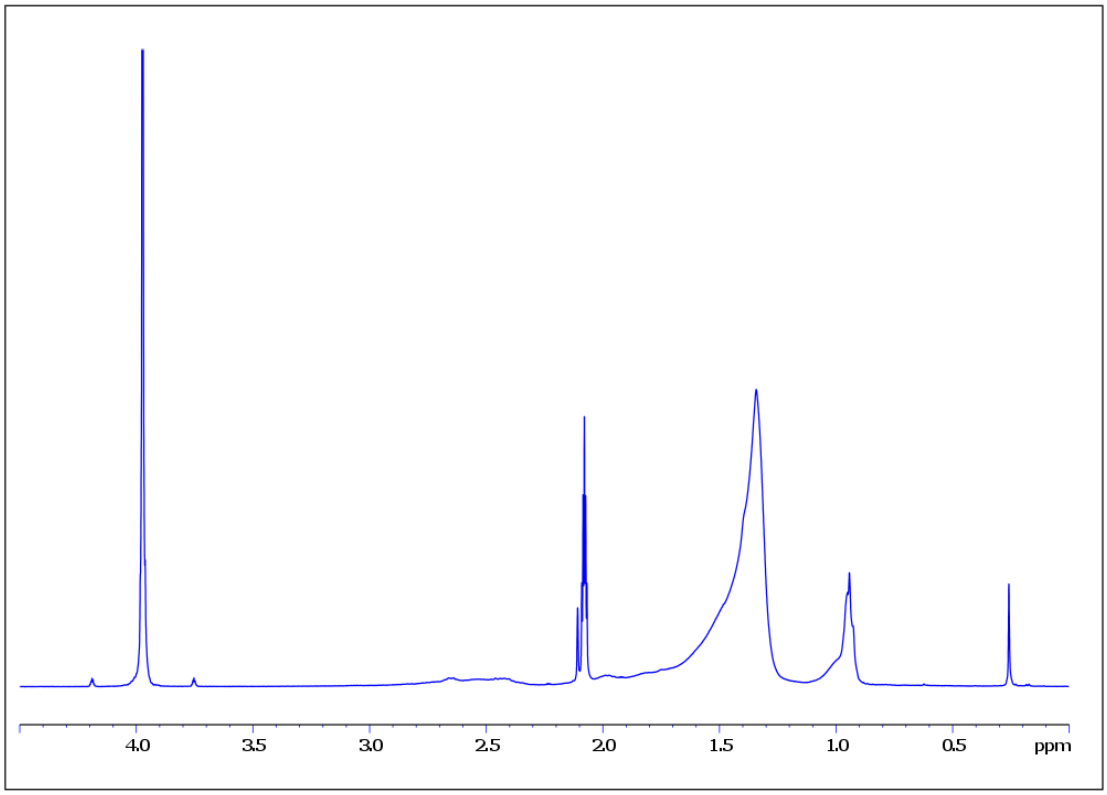

Figure 2.6 ^{1}HNMR myristate ligand population calculated from both the CH_2 and CH_3

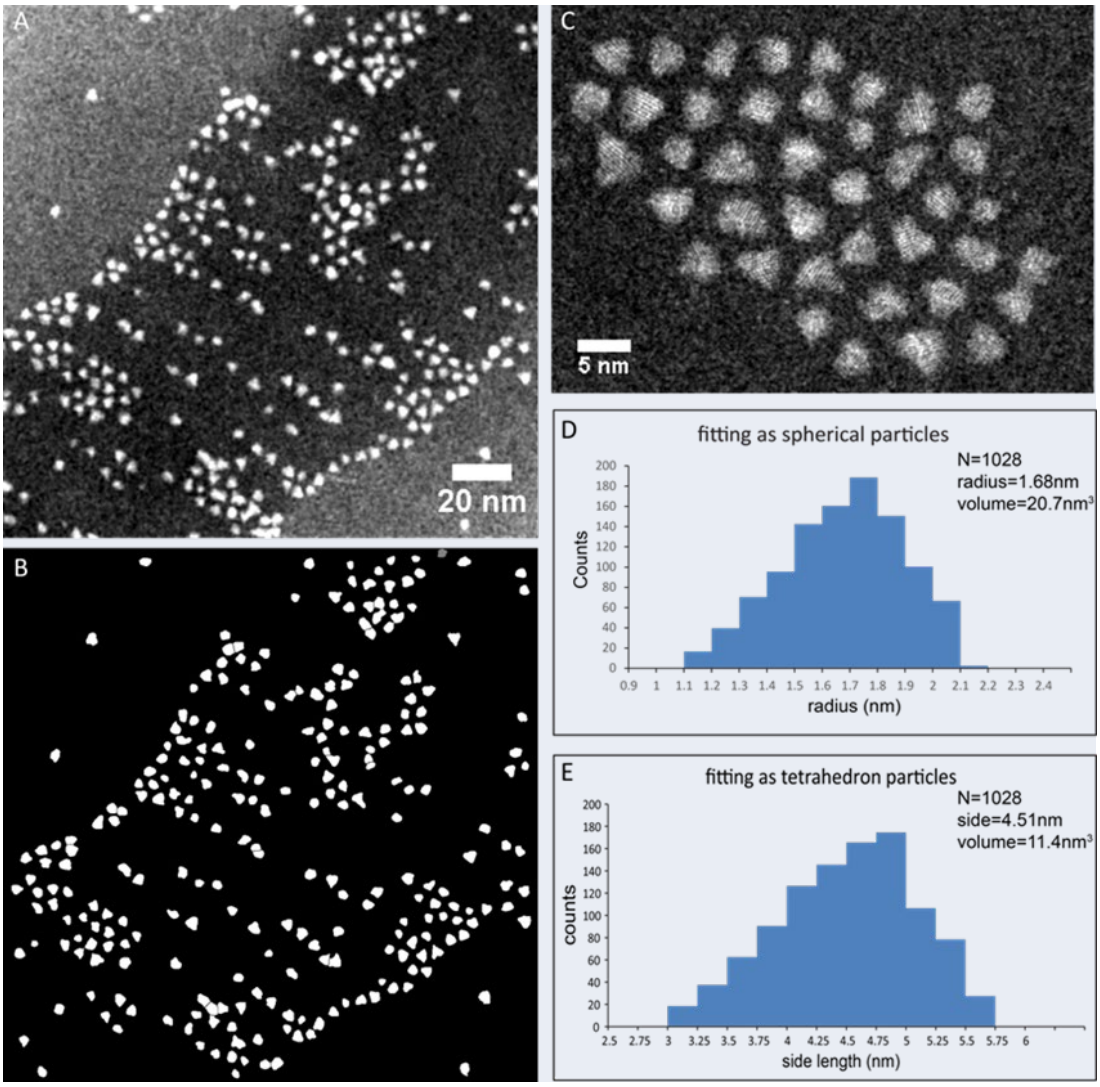

Figure 2.7 STEM image of InP particles (A) and image mask of region used for size analysis (B). Magnified image of particles (C). Size histograms fitting the particles as spheres (D) and tetrahedron (E).

Chapter 3

Purification and in-situ ligand exchange of metal-carboxylate treated fluorescent InP quantum dots via gel permeation chromatography

3.1 Introduction

Colloidal semiconductor quantum dots (QDs) have received considerable attention due to their low cost of fabrication, large extinction coefficients, and the ability to tune their optoelectronic properties based on size and composition. CdSe QDs have been the most well-characterized system to date; however, as more technologies become commercially viable, concerns about environmental contamination and toxicity and associated regulatory pressure can limit the use of cadmium-based materials. For example, in the EU there are already regulations in place that limit the use of cadmium- and lead-based materials in electrical and electronic equipment, and because of these regulations, there is a desire to move away from cadmium-based systems.

InP QDs have received increasing attention over the past few years as alternatives to the more well-characterized CdSe and PbS QD systems because of the range of visible and near-infrared effective bandgaps that can be accessed.[10] Still, numerous challenges are associated with InP QDs. In addition to their rapid oxidation in air, InP QDs have suffered from low-photoluminescence (PL) quantum yields (QYs) that decrease their viability for use in optoelectronic applications.[11] In previous QD systems, the creation of a core/shell structure has been used to improve the QY as well as improve air stability.

The coating of a shell material with a larger band gap passivates surface dangling bonds as well as localizes the wave function to the core, spatially separating the core from the environment to reduce its influence on the optoelectronic properties. The growth of cadmium sulfide (CdS) and zinc sulfide (ZnS) shells, in particular, have both been observed to improve the photoluminescence of InP QDs and many other nanocrystal materials.[12–17]

One method that has been used in the synthesis of shells onto the QD core is successive ionic layer and adhesion reaction (SILAR), which utilizes alternating precursor additions to saturate the surface sequentially in an attempt to force conformal growth onto the core.[18,19] By carefully controlling the precursor injections so that the reaction is self-limiting, side reactions that generate small particles of the shell material can be minimized.[20] This self-limiting reaction has led to the successful creation of many core/shell systems. In the case of InP QDs, it was found that in the stepwise synthesis of ZnS and CdS shells onto the core, during the initial addition of the Lewis acid M^{2+} (M = Zn, Cd; introduced as oleate salts), a hypsochromic and bathochromic shift occurs for Zn^{2+} and Cd^{2+}, respectively, and an increase in QY is observed (Figure 3.1). This increase in the QY was attributed to the surface passivation of dangling phosphorus bonds.[21] The ability to tune the absorbance and emission spectra based on the amount of M^{2+} added without a substantial change in particle size provides a unique opportunity to access a wide spectral range without modifying the core synthesis. If this initial M^{2+} layer is stable to further processing conditions (purification and ligand exchange) that are frequently performed in pursuit of applications, it could provide an interesting alternative to full-

shell synthesis while also offering a route to highly emissive QDs with decreased or eliminated Cd content.

We report an investigation into the stability of this surface M^{2+} layer by measuring the change in M^{2+} content and QY after purification via gel permeation chromatography as well as after exposure to ambient conditions. Gel permeation chromatography (GPC), a type of anhydrous size-exclusion chromatography, has been established over the past few years as a repeatable method to purify QD solutions, removing synthetic impurities and weakly bound ligands without causing aggregation or etching.[8,22] Furthermore, by taking advantage of the differing rates at which small and large molecules flow through the chromatography column, it is possible to design a system in which a ligand-exchange reaction can occur during the time the QDs traverse the column.[23] Here we use this "on-column" exchange to switch the native oleate ligands coordinated to the Lewis acid to hexylphosphonate ligands in an attempt to improve the air stability of the InP QDs.

3.2 Results and Discussion

We have previously demonstrated purification by GPC as a reproducible method to remove synthetic impurities and weakly associated ligands from InP QDs.[23] Furthermore, we have demonstrated that GPC selectively removes weakly bound ligands that can modulate quantum yield in CdSe/CdZnS core/shell QDs.[2] The InP QDs samples here were prepared with myristate ligands and treated with Zn^{2+} or Cd^{2+} as described previously.[21] Accordingly, it is key to test whether the metal carboxylate ligands are separated by GPC purification and determine the influence purification has on the QY. Ligand populations in QD samples can be monitored by ^{1}H and ^{31}P NMR spectroscopy,[9]

and UV–visible absorption spectroscopy can be used to normalize for differences in QD concentration and to assign approximate QD concentration values if extinction coefficients are known. The purifications described here were conducted at an approximate QD concentration of 25 μM based on reported extinction coefficients for InP QDs of comparable size[24,25] and were performed in anhydrous toluene (AT) under air-free conditions. As shown by the ^{1}H NMR spectra in Figure 3.2, purification of the cadmium-oleate-coated InP (Cd-InP) QDs shows a large decrease in olefin-containing impurities such as 1-octadecene. The broad resonance at ∼5.5 ppm is assigned to the olefin protons of the strongly bound cadmium oleate ligands that remain present after purification. In addition to the ^{1}H NMR spectra, we monitored changes in absorbance and emission spectra (Figure 3.3), and after 1 week no changes are observed in the optical spectra. Inductively coupled plasma mass spectrometry (ICP–MS) was run on aliquots sampled before and after purification to check if GPC purification was decreasing the cadmium content relative to indium (Figure 3.4). After GPC purification, there was no observable change in the Cd/In ratio, indicating that purification did not remove the cadmium oleate bound to the QDs. In the case of the zinc-oleate-treated InP (Zn-InP) QDs, purification by GPC causes a small decrease in the Zn/In ratio (Figure 3.4). The QY was monitored before and after GPC purification (Figure 3.5), and for the Zn-InP QDs there was a small decrease in the QY after GPC purification. In both cases there was minimal change in the low-energy absorption and emission peak positions after purification. The purification results can be explained by a diminished binding strength of Zn carboxylate to the InP surface relative to Cd in toluene solvent. We note that in a previous study of SILAR shell growth on CdSe, a diminished synthetic yield for ZnS

growth from $Zn(oleate)_2$ was seen compared with CdS growth from $Cd(oleate)_2$, consistent with a comparatively weak association of $Zn(oleate)_2$ to the CdSe surface at the reaction temperature.[26] Although not directly comparable, these two results suggest that binding of Lewis acidic metal salts to InP and CdSe surfaces may follow similar trends. Importantly, the retention of M^{2+} during GPC purification indicates that exposure of carboxylate-capped InP QDs to metal salts can yield stable colloidal complexes whose subsequent chemistry in the presence of specific reagents can be investigated further. Similar to the absorbance and emission changes due to the addition of cadmium and zinc oleate to InP, it has been shown in CdSe clusters that with the addition of the Lewis acid cadmium benzoate the QY increases and a large bathochromic shift in the absorption and emission peaks occurs.[27] Etching of Lewis acid "Z-type" ligands can be achieved with the addition of nucleophilic amine ligands.[28] For example, N,N,N′,N′-tetramethyl-ethylene-1,2-diamine (TMEDA), a Lewis base that chelates such ligands in solution, has been demonstrated as a means to decrease the amount of Lewis acidic ligand coverage on the QD surface.[27,29] The bathochromic shift in the optical spectra was shown to be reversible through etching of the Z-type cadmium carboxylates with TMEDA. The origin of the increased QY and bathochromic shift were attributed to passivation of nonradiative trap states and exciton delocalization into the ligand monolayer through hybrid orbitals that are characteristic of both the nanocrystal and ligand. The exact role of cadmium carboxylate and zinc carboxylate in altering the optical properties of InP has seen conflicting reports, but arguments regarding impacts on exciton localization appear most consistent with our experimental data.[12,30]

To test whether the M^{2+} is surface-bound or incorporated into the InP crystal structure, chemical etching of the QDs with TMEDA was performed. Etching of InP QDs has been performed previously with HF and with ionic liquids to create luminescent particles.[24,31] We hypothesize that if the M^{2+} is, in fact, diffusing into the InP lattice, etching with TMEDA will not alter the metal carboxylate content on short time scales. Previous etching experiments monitored changes in QY upon the addition of TMEDA; however, the byproducts formed could not be separated.[21] Here etching of Zn-InP QDs was performed by preloading TMEDA onto the GPC column before the addition of the QD solution. This "on-column" reaction will tend to separate any small-molecule products extruded from the QD surface. ^{1}H NMR of the collected eluent showed evidence of bound olefin remaining (Figure 3.6). A shift in the peak position in the absorbance spectra after the on-column etch compared with a GPC-purified sample was observed, however, which is an indication of the increased removal of zinc in the presence of TMEDA (Figure 3.7). We also examined the displacement of zinc oleate from the surface of the Zn-InP QDs by titrating TMEDA into a Zn-InP QD solution and monitoring changes in the ^{1}H NMR spectrum (Figure 3.8). Olefin protons of oleate ligands that are attached to the QD appear as a broad peak in the NMR due to the slow tumbling, whereas unbound oleate appears as sharp peaks. By monitoring the shift from bound to unbound oleate upon the addition of TMEDA there is evident decrease in the bound olefin signal. This has been demonstrated previously in the etching of Cd-rich CdSe with TMEDA and in the stripping of anionic ligands from PbSe QDs through the formation of BF3 adducts.[29,32] Here we found that the ligand displacement reached equilibrium on the order of 5 min or less, and this rapid exchange lends support to the metal carboxylate dopants

being localized to the surface rather than dispersed through the nanocrystal. Although rapid ion exchange has been observed in chalcogenide QDs,[33] temperature-dependent diffusion studies for Zn in bulk InP report slow diffusion. The diffusion constant D has been reported to vary as $D = D_0 \exp(-Ea/k_BT)$ with $D_0 = 9 \times 10^{-2}$ cm^2/s with Ea = 1.52 eV.[34] These values predict $D \approx 10^{-27}$ cm^2/s at 300 K. For comparison, diffusion out of a sphere[35] with the nanocrystal radius (~1.5 nm), on the equilibration time scale observed in the ^1H NMR (300 s), would require a diffusion constant $D \approx 10^{-17}$ cm^2/s, a difference of 10 orders of magnitude. From this analysis, we conclude that at least a large portion of the Zn content in the fluorescent Zn-InP QDs is localized to the surface. InP particles rapidly oxidize in air, which is detrimental to the optical properties of the QDs. In an attempt to improve the air stability of the InP particles, we utilized an in situ ligand exchange on the GPC column[23] to switch the carboxylate ligands to phosphonate ligands. In CdSe QDs, it has been demonstrated that phosphonate ligands have a stronger binding to the surface than carboxylate ligands.[36,37] We hypothesize that this increased binding strength could provide a more protective ligand layer to inhibit oxidation in the case of InP QDs. To achieve exchange of carboxylate to phosphonate on the Cd-InP sample, we introduced a solution of hexylphosphonic acid (HPA) in AT. To scavenge excess protons from the phosphonic acid, diisopropyl ethyl amine (DIPEA) was introduced as well. This solution was preloaded onto a 20 cm high GPC column, followed by a section of neat AT and then the Cd-InP QDs. The exchange reaction went to completion, as seen in the near-complete decrease in olefin-containing species in the ^1H NMR (Figure 3.9), with only a minor peak remaining that we assign to a small amount of unbound oleate species remaining in the solution. With sufficient column length, it is conceivable that the

byproducts can be completely removed from the QD fraction in a single run, but space constraints in the glovebox prohibited packing of a longer column. To further investigate this ligand-exchange reaction, we conducted it in a more traditional process in which initial purification, exposure to the new ligand, and subsequent purification to remove byproducts from the exchanged particles are conducted as discrete steps. We performed this "normal" ligand exchange on GPC-purified Cd-InP particles, and evidence of the complete exchange and complete removal of oleate products can be seen in the ^{1}H NMR (Figures 3.10 and 3.11). To confirm that the exchange was replacing the carboxylate ligands with phosphonate ligands on the M^{2+} rather than displacing metal oleate or phosphonate products (Figure 3.12), the Cd/In ratio was compared before and after the exchange through ICP–MS (Figure 3.13). The Cd/In ratio does not change significantly after the exchange reaction when compared with the GPC-purified, but unexchanged, samples. This result combined with the decrease in bound olefin in the NMR provides strong evidence of X-type ligand exchange accompanied by proton transfer from HPA to oleate/DIPEA. We note that the surface of the Cd-InP dots prior to exchange is composed of a combination of myristate ligands present after InP synthesis and oleate ligands used to balance the M^{2+} Lewis acid. The X-type ligand exchange replaces not only the oleate ligands but also the myristate ligands, as integration of the aliphatic region indicates a CH_3/CH_2 ratio corresponding to purely hexylphosphonate ligands present at the surface. The oleic acid and myristic acid byproducts of this exchange can be completely removed by GPC in toluene. Before considering oxidation on exposure to ambient atmosphere, it is important to consider the intrinsic stability of the carboxylate- and phosphonate-capped QDs under air-free conditions. Cros-Gagneux et al. reported that oxidation at the surface

of InP QDs can occur through decarboxylative coupling that provides the conditions for oxidation in the absence of air.[38] In our own investigation of the present InP QDs and M^{2+}-coated samples prior to ligand exchange, we find no evidence of oxidation in ^{1}H–^{31}P cross-polarization NMR spectra (Figure 3.14). X-ray emission spectroscopy (Figures 3.15 and 3.16) showed only 10% phosphorus oxidation, which is attributed to the sample preparation as the samples were exposed to air briefly before insertion into spectrometer; this offers additional evidence that oxidation of phosphorus in these materials as prepared is minimal.

The stability of metal-ion-treated InP particles following purification and ligand exchange and upon subsequent air exposure was monitored by changes in the absorbance and emission spectra as well as in changes to QY (Figure 3.17). Specifically, the QY of Cd-InP samples was recorded under an inert atmosphere, after bubbling with ambient atmosphere for 20 min, and after 1 week of storage sealed under an ambient atmosphere following bubbling. The unpurified stock Cd-InP sample does not show any shift in the absorbance spectra after 1 week of storage in an ambient environment but does, however, see a decrease in emission intensity. This is the same for the QDs that were purified by GPC. As noted above in Figure 3.3, a control sample of Cd-InP QDs purified by GPC and kept under an inert atmosphere showed no apparent change in either the absorbance or emission spectrum. In the case of the phosphonate-capped QDs the absorbance spectrum peak blue shifts by 50 nm and the emission peak blue shifts by 30 nm over a week of ambient exposure with significant change appearing within 20 min (Figure 3.17 and Figure 3.18), a shift that exceeds the initial red shift on introduction of Cd and is thus indicative of erosion of the QD core. The QY of the exchanged dots was also measured

immediately after the exchange and after 1 week of storage under ambient conditions. The QY is reduced from 20% immediately after exchange to 8% after 1 week. This change is similar to the value of the initial Cd-InP sample with carboxylate ligands in which over 1 week of air exposure, the stock solution QY decreased from 26 to 10%. The GPC-purified, carboxylate-capped sample saw a decrease in the QY from 26 to 9% after 1 week of air exposure. In summary, the ligand exchange to phosphonate ligands did not improve the air stability of the M^{2+}-coated particles, and this remains an issue that needs to be resolved for these particles to serve as luminescent alternatives to core/shell particles in many applications. The addition of M^{2+} (Cd, Zn) to InP QDs causes a bathochromic/hypsochromic shift in the absorbance and emission spectra and leads to an increase in the QY. GPC purification of these particles leads to a minimal change in both the QY and the ratio of M^{2+}/In. The M^{2+}-InP QDs could be made to undergo two different types of ligand-exchange reactions. In particular, the metal carboxylate was successfully etched and separated through exposure to TMEDA, a process that can be described as reactive displacement of a "Z-type" ligand, and the rate of this reaction suggests that the metal is surface bound rather than alloyed into the crystal lattice. Additionally, the use of GPC allowed for successful ligand exchange of the initial oleate ligands to hexylphosphonate in stepwise and in situ processes, indicating that X-type exchange can be accomplished without displacing the Lewis-acidic metals. This is, to our knowledge, the first demonstration of complete X-type ligand exchange on InP QDs; similar transformations have recently been carried out for InP magic size clusters.[39] Although fluorescence under air-free conditions was maintained, this ligand exchange did not improve the air stability of the rapidly oxidizing InP particles. Nonetheless, the

observation that strongly bound complexes can be achieved by the addition of Lewis acidic metal salts to InP QDs suggests that this approach, together with subsequent ligand exchange, is an important tool for improving material performance and facilitating technological translation.

3.3 Materials and Methods

All chemicals were used as received without further purification. Anhydrous toluene 99.8% was purchased from Alfa Aesar, d8-toluene 99.5% was purchased from Cambridge Isotope Laboratories, Bio Beads S-X1 was purchased from Bio Rad, hexylphosphonic acid was purchased from PCI, N,N,N′,N′-tetramethylethylenediamine 99% and ferrocene 98% were purchased from Acros Organics, diisopropylethylamine and Rhodamine 590 were purchased from Exciton, and ethanol 200 proof was purchased from Decon. ^{1}H NMR spectra were recorded on Bruker Avance III 400 MHz. The optical absorption spectrum was recorded using a Thermo Scientific Evolution Array UV–visible spectrophotometer with toluene as the solvent as well as the blank in a 1 cm path quartz cuvette. Fluorescence spectra of QD and R590 dye were taken under identical spectrometer conditions on a Varian fluorescence spectrometer in triplicate and averaged. Inductively couple plasma mass spectrometry (ICP–MS) spectra were recorded on a Thermo-Finnigan Element XR ICP–MS.

Synthesis of Zn-InP and Cd-InP. Metal-coated InP QDs were synthesized following the procedure by Stein and Cossairt.[21] In brief, zinc oleate (cadmium oleate) was added to a solution of InP QDs (approximately 1:2 Zn/In (2:1 Cd/In) molar ratio) and stirred at 200 °C for 3 h, after which the solution was cooled to room temperature, and the 1-octadecene was removed by distillation under vacuum.

Purification of Zn-InP and Cd-InP. Three mL of Zn-InP QDs in pentane was removed in a sealed vial and pumped dry using a Schlenk line. The dried sample was transferred back into nitrogen glovebox and dissolved in 3 mL of AT and filtered through a 0.2 μm PTFE syringe filter. One mL of this filtered solution was separated and distributed into three vials for ICP–MS measurements. The QY was measured by taking 50 μL of the Zn-InP solution into 2.5 mL of AT. This was found to yield an absorbance at the λmax below 0.1 A.U. and was done to reduce possible reabsorption affects. The remaining 2 mL of filtered Zn-InP was reduced in volume on a Schlenk line to ~0.8 mL for injection onto the GPC column. An eluted fraction of ~2 mL containing QDs was collected. The QY was recorded after purification using 50 μL in 2.5 mL of AT. The remaining Zn-InP solution was split into three separate vials for ICP–MS. Samples were prepared for ICP–MS by evacuation to dryness, followed by digestion with aqueous HNO_3. The same procedure was followed for the Cd-InP sample.

Zn-InP Etch with TMEDA. ~20 nmol Zn-InP was removed from the vial and injected onto the chromatography column, and the collected sample was pumped dry and redissolved in 0.8 mL of d8-toluene. ^{1}H NMR was run on the initial stock solution; then, 50 equiv. of TMEDA relative to the Zn on the surface was added and the ^{1}H NMR spectra were recorded again. The addition of 20 equiv. of TMEDA was titrated into the NMR tube, and after agitating to mix, the spectra were recorded again, until a total of 210 equiv. of TMEDA was added to a final [TMEDA] of 2.64 M (volume fraction of 40%).

Phosphonate Ligand Exchange. Hexylphosphonic acid (6 mg) and diisopropylethylamine (5 μL) were dissolved in 4 mL of AT, and the resultant solution was injected onto the GPC column. This solution was followed by 2 mL of neat AT, after

which the Cd-InP solution was injected (~20 nmol). A 2 mL fraction of the eluent, containing the QD band, was collected. QY was measured after the exchange using 100 μL of QD solution in 2.5 mL of AT. The remaining 1.9 mL solution was pumped dry and dissolved in d8-toluene with internal standard of ferrocene (2 mg). The ^{1}H NMR spectrum was recorded.

Cd-InP Stability Test. ~18 nmol of Cd-InP QDs was used for each trial and was directly injected onto the GPC column. In each case ~2 mL of QD solution was collected from the column and the QY was measured by taking 100 μL of the solution diluted in 2.5 mL of toluene. The samples were bubbled with ambient atmosphere for 20 min after which the QY was recorded again. The samples were then stored in the dark to decrease the possibility of photo-oxidation, and after 1 week, the QY was once again recorded. The collected samples were then digested with HNO_3 and the Cd and In content was measured.

3.4 Figures

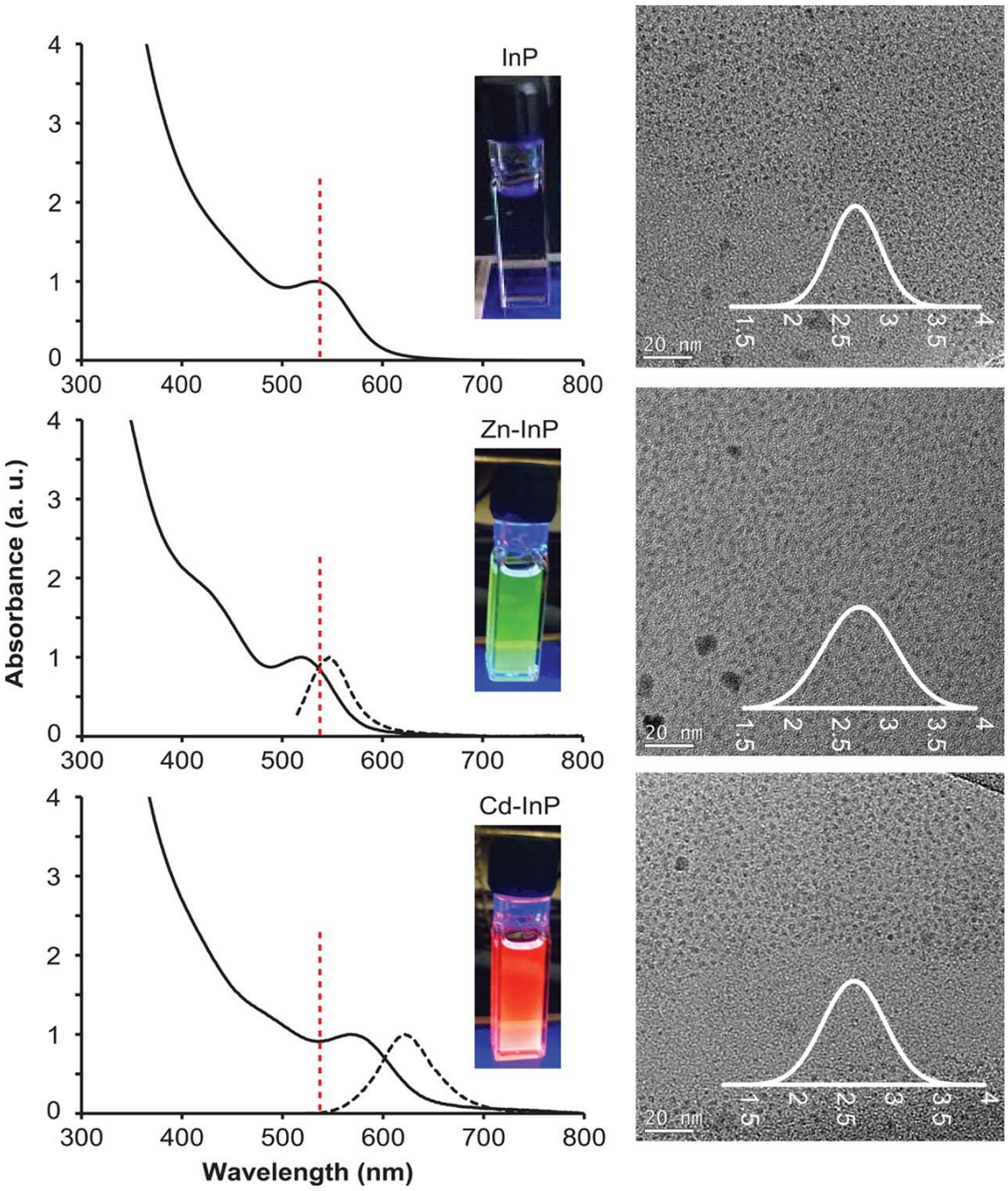

Figure 3.1 Absorbance (solid) and PL (dashed) spectra of InP, Zn-InP, and Cd-InP (left) TEM (right).

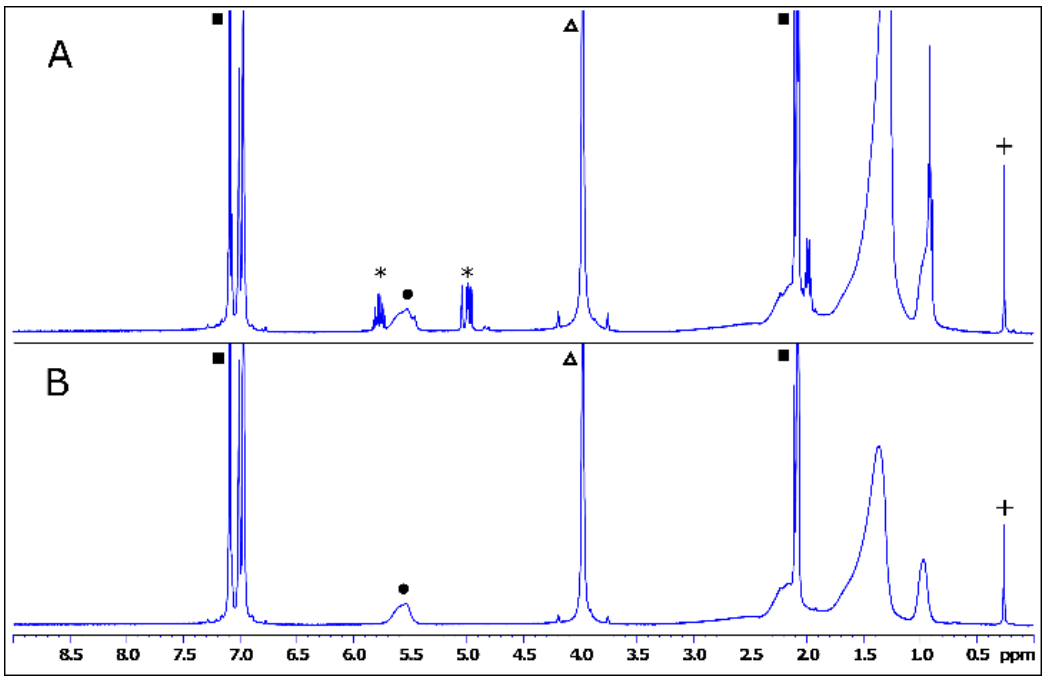

Figure 3.2 ^{1}H NMR (A) before GPC purification and (B) after GPC purification of cadmium-oleate-coated InP (Cd-InP) QDs showing a large decrease in olefin-containing impurities such as 1-octadecene (*) while strongly bound oleate ligands remain (●). Peaks associated with the toluene solvent (■), ferrocene internal standard (△), and TMS (+) are also visible.

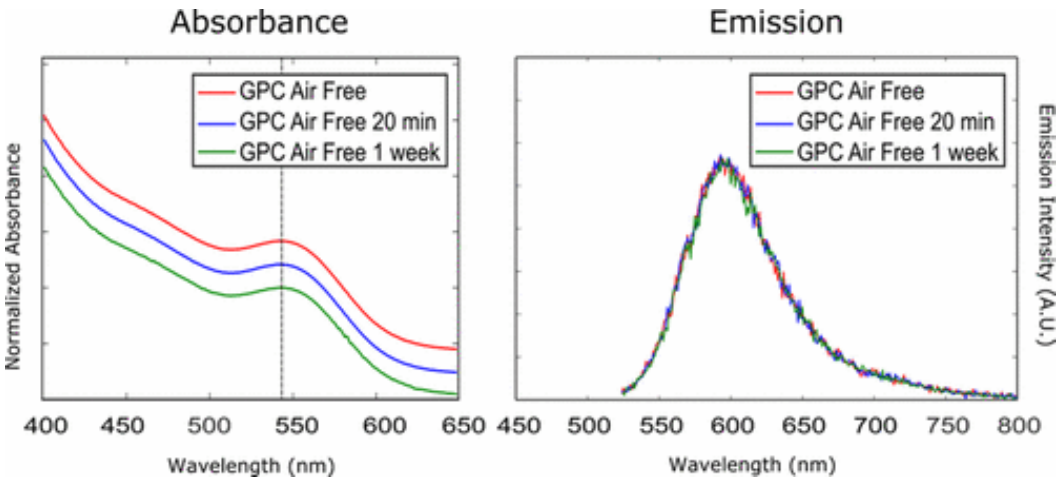

Figure 3.3 Stability of GPC purified Cd-InP QD samples kept under inert atmosphere, indicating no change in the absorbance (left) and emission (right) after 1 week.

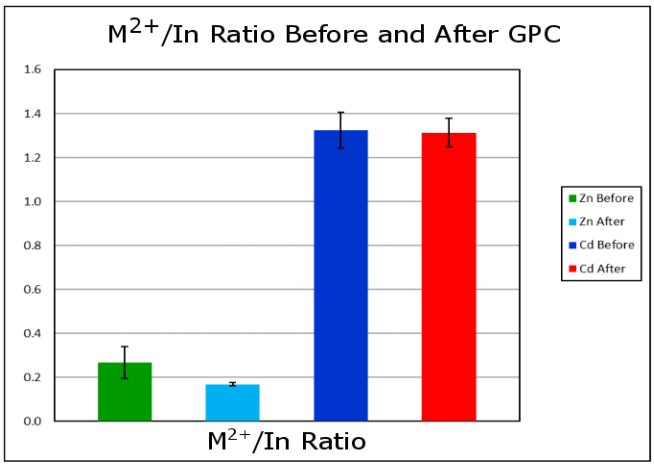

Figure 3.4 M^{2+}/In ratio before and after GPC as determined by ICP-MS.

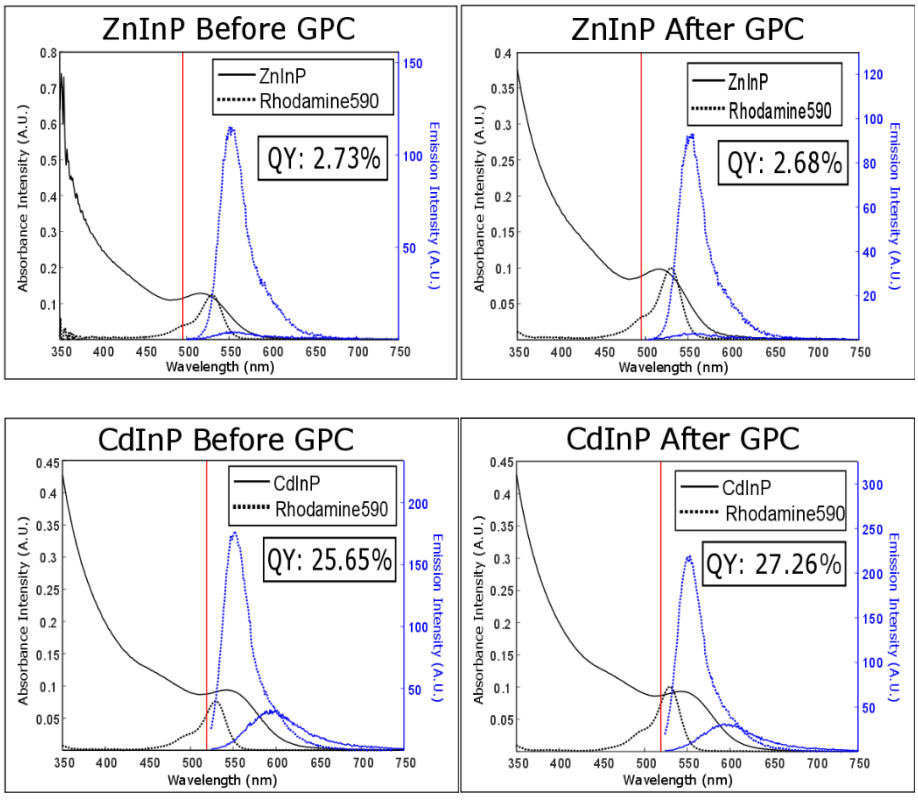

Figure 3.5 Absorbance and emission spectra before and after GPC for $Zn^{2+}$and Cd^{2+} samples with Rhodamine 590 dye reference. Red line indicates excitation wavelength for the emission measurements.

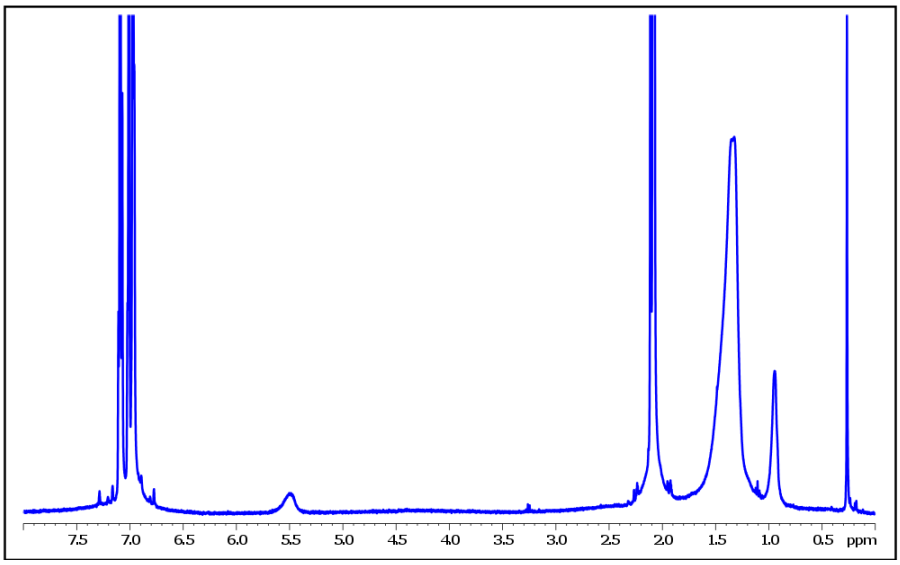

Figure 3.6 ^{1}HNMR of sample that underwent on-column etch with TMEDA. Evidence of incomplete etch shown by the presence of olefin protons ~5.5 ppm.

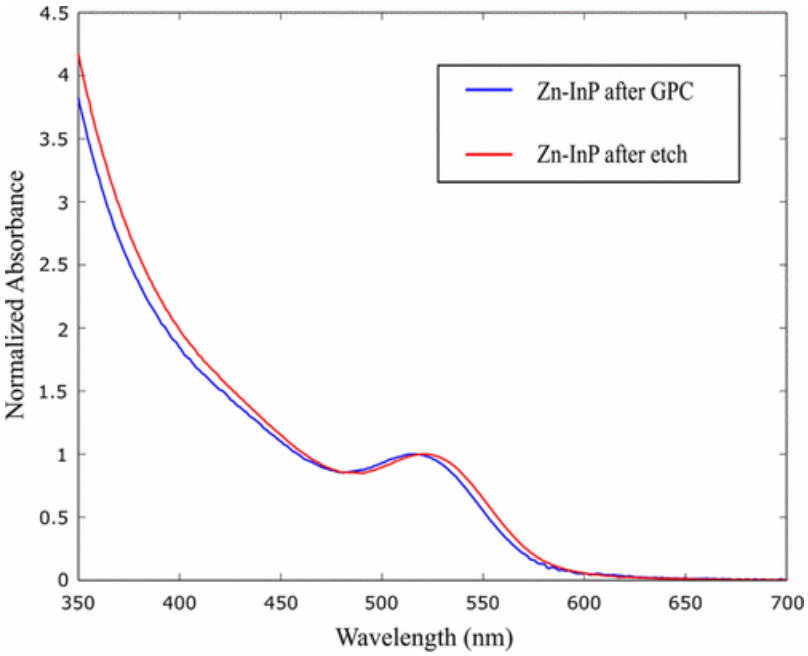

Figure 3.7 Normalized absorbance spectra after purification by GPC and after on-column etching with TMEDA showing a red shift in the low-energy excitonic transition.

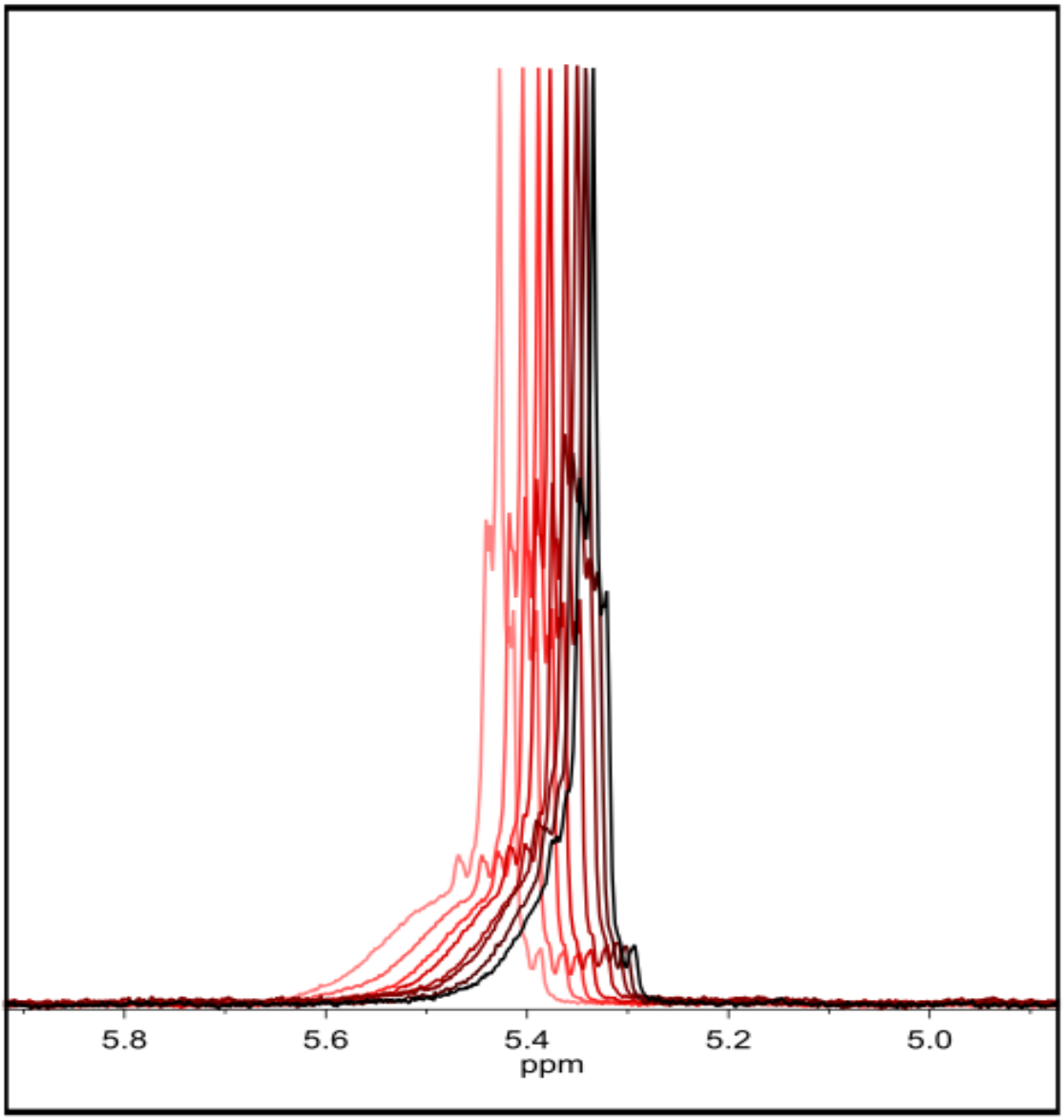

Figure 3.8 Olefin region of ^{1}H NMR during titration of TMEDA into Zn-InP QD solution. Decrease in the broad resonance associated with bound oleate and increase in sharp resonances indicates and increase in free oleate species in solution.

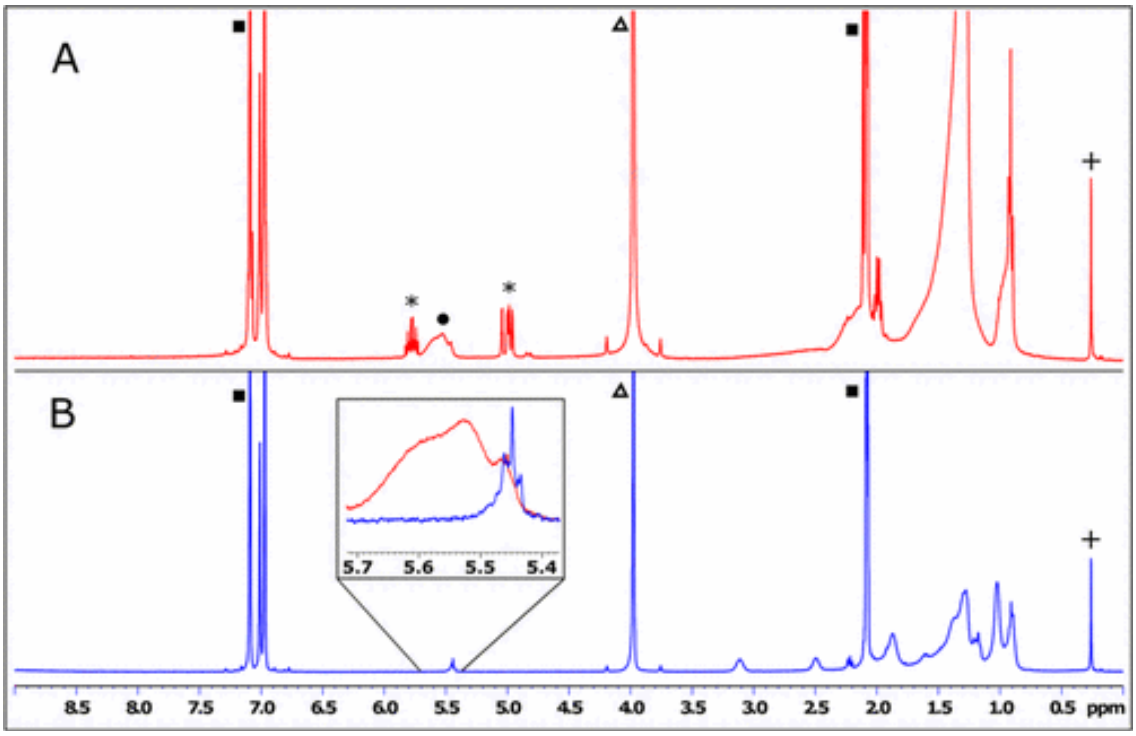

Figure 3.9 ^{1}H NMR of Cd-InP (A) before exchange reaction (1-octadecene (*), oleate (●), toluene (■), ferrocene (△)) and (B) after on-column exchange with hexylphosphonic acid. Inset in panel B compares oleate resonances before (red) and after (blue) ligand exchange. After exchange, only sharp resonances near 5.45 ppm, indicative of free oleate, are seen. Although the reaction is complete, incomplete separation of byproducts is evidenced by the residual free oleate and DIPEA (peaks ≈ 2.5, 3.1 ppm).

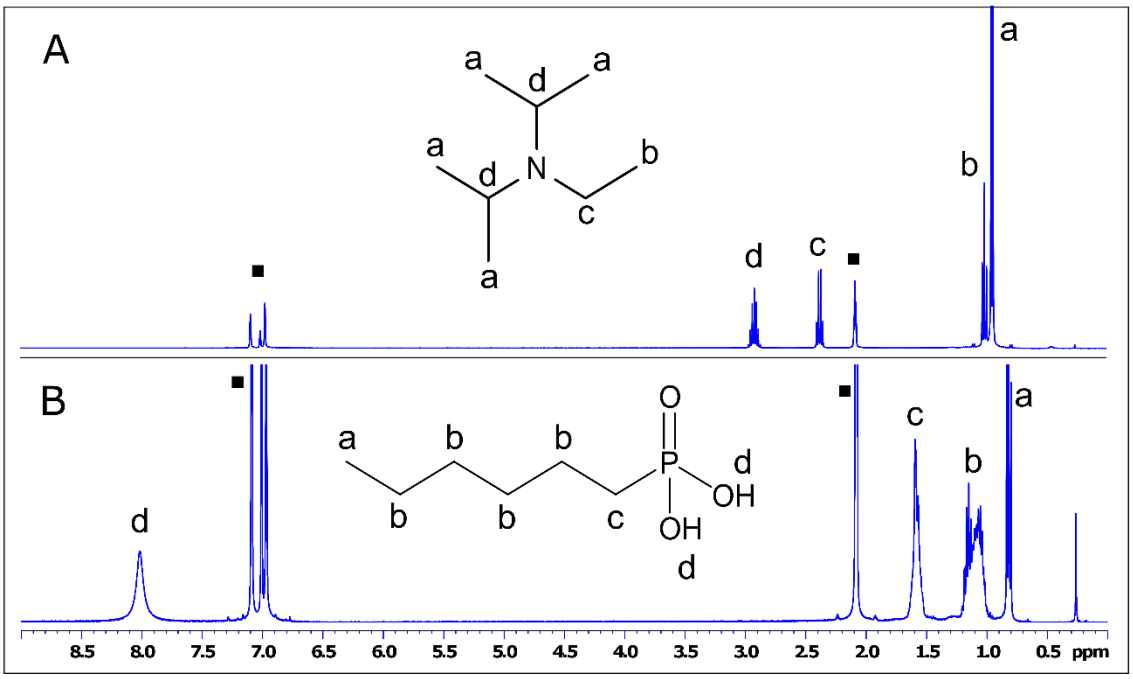

Figure 3.10 [1]HNMR of ligand exchange reactants (A) DIPEA and(B) HPA in d8-toluene. Peaks associated with the toluene solvent (▪) are also visible.

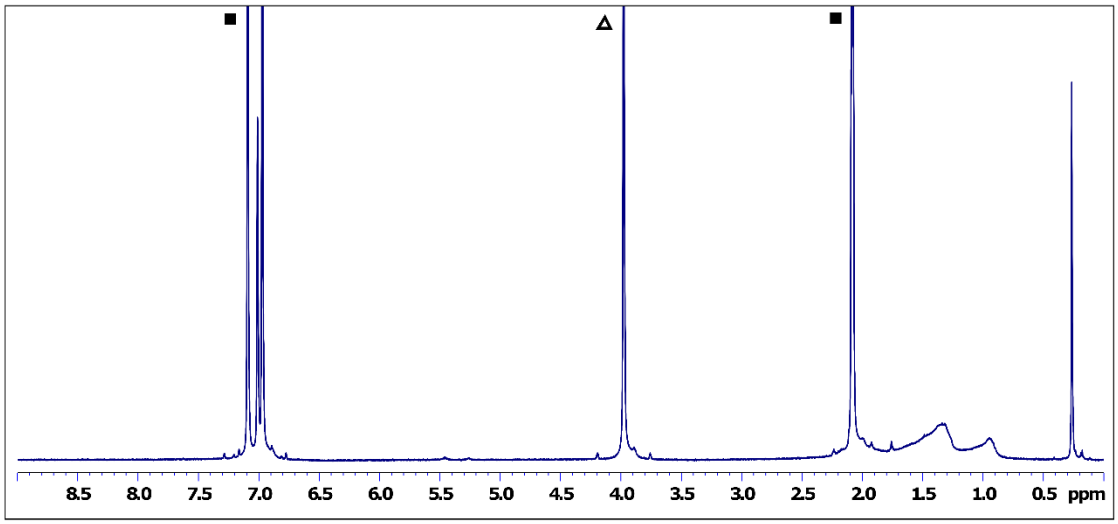

Figure 3.11 [1]HNMR of Cd-InP after “normal” exchange. Peaks associated with the toluene solvent (▪) and ferrocene internal standard (Δ).

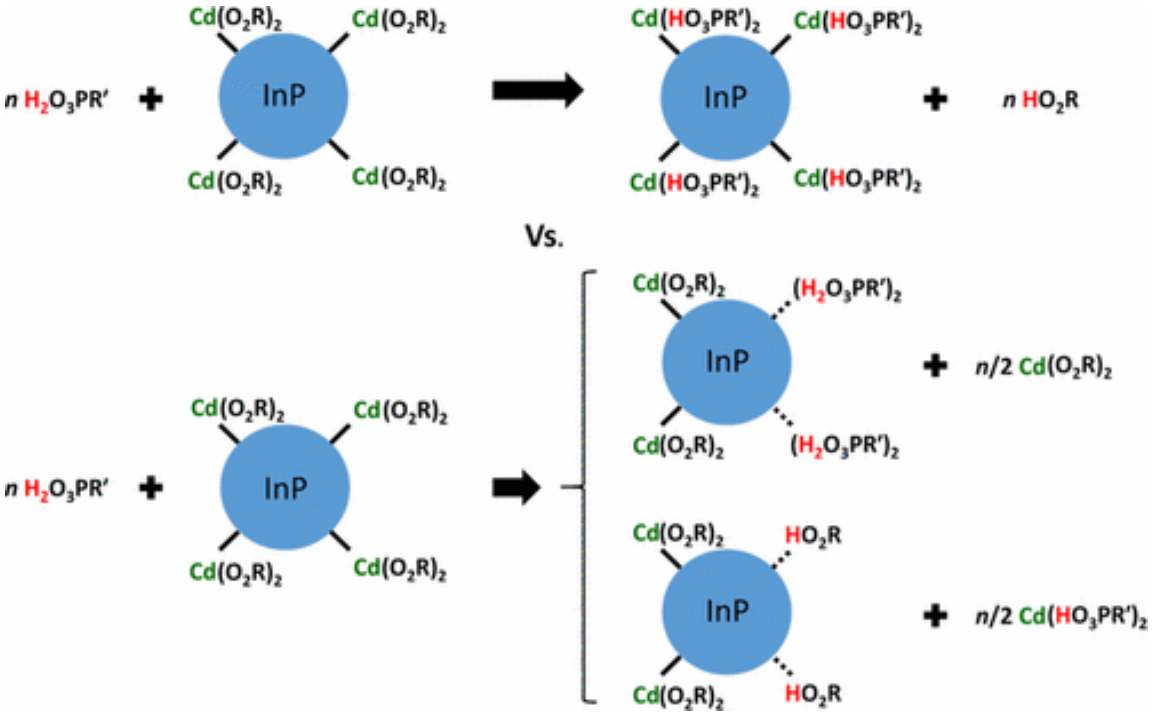

Figure 3.12 Observed X-type exchange versus possible displacement reactions at the M^{2+}-InP surface

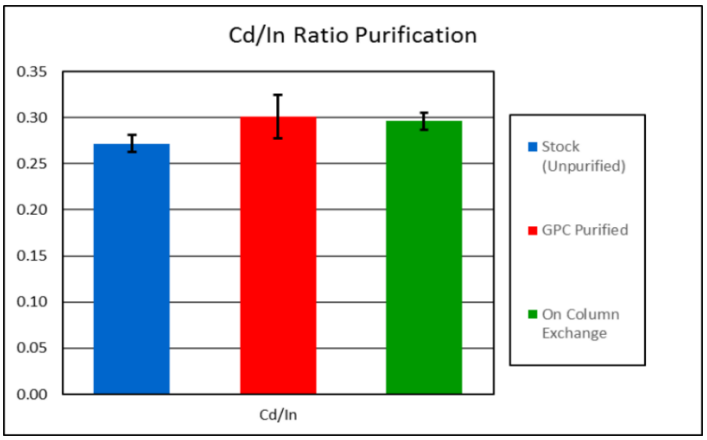

Figure 3.13 Changes in Cd/In ratio after purification and ligand exchange determined by ICP-MS. Note that this experiment used a different Cd-InP QD sample than was used in Figure 3.4

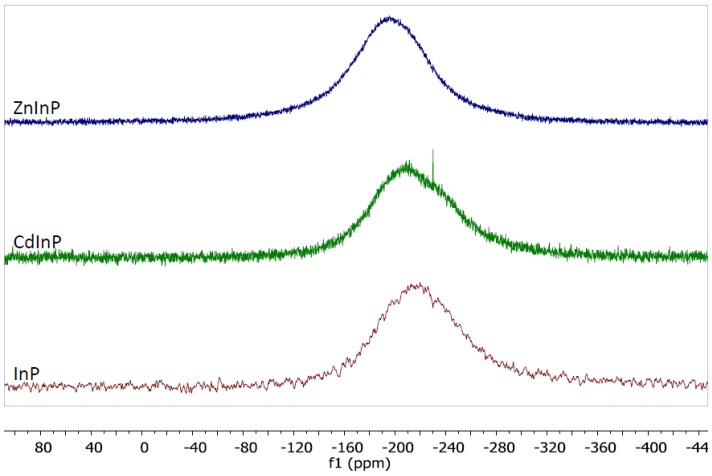

Figure 3.14 ^{1}H-^{31}P cross polarization NMR does not show any evidence of oxidation of the InP particles after synthesis ($InPO_x$ peak at 0 ppm).[38]

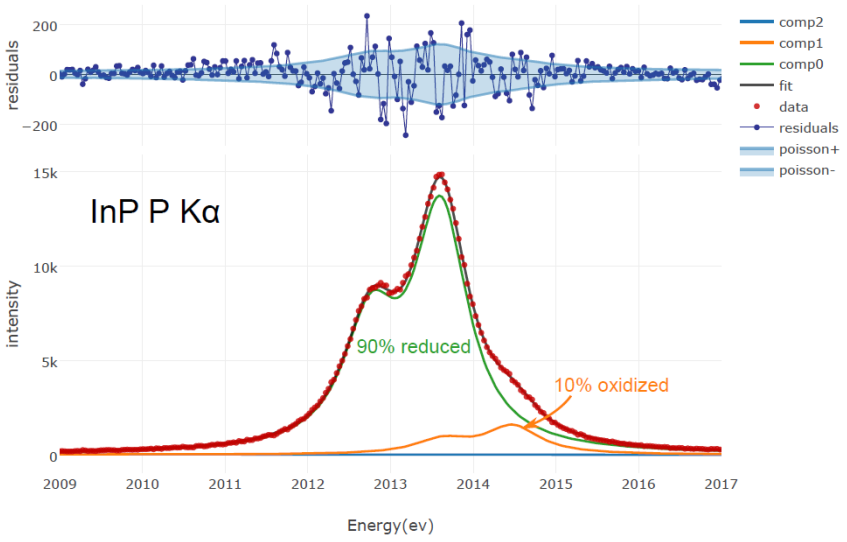

Figure 3.15 X-ray emission spectrum collected on a film of InP QDs. Linear combination fits of reference spectra to the P K_α spectra for InP QDs showing the relative proportions of oxidation states of phosphorous. The lower energy doublet corresponds to a reduced oxidation state (P^{3-}), while the higher energy doublet represents a highly oxidized state ($P^{3+/5+}$)

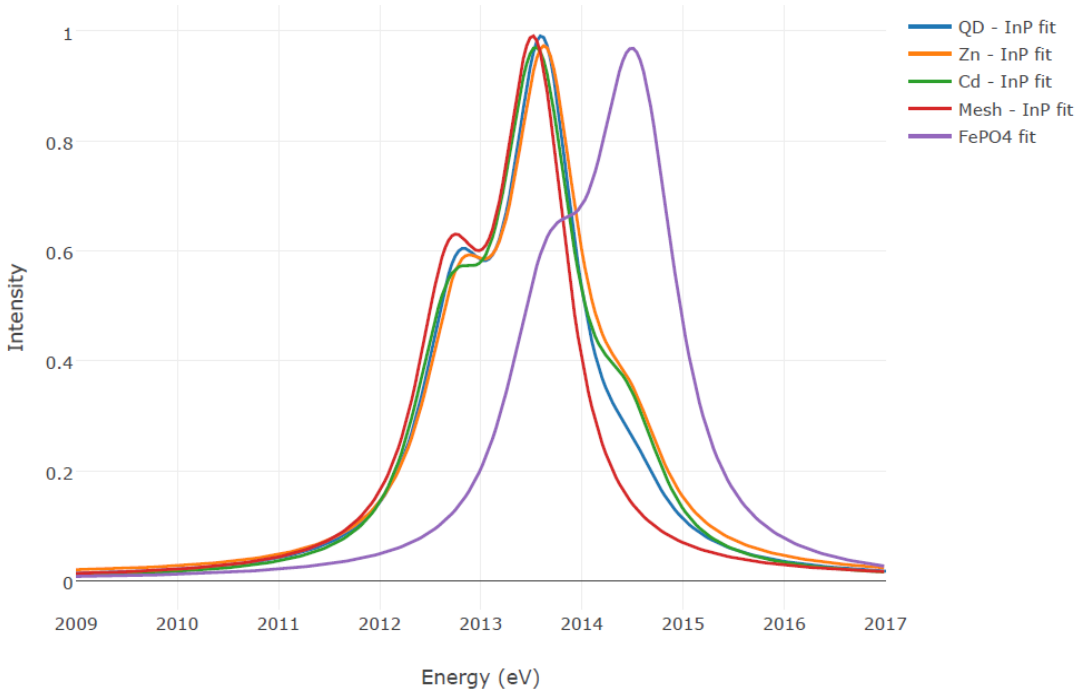

Figure 3.16 Overlay of X-ray emission spectra collected on InP, Cd-InP, Zn-InP QDs comparing the overall oxidized P content. Bulk InP mesh (red) and $FePO_4$(purple) were used as references to fit the oxidized P content measured in the QDs. Although the introduction of Zn/Cd increased the total oxidized P, it is minor and not dependent on metal identity.

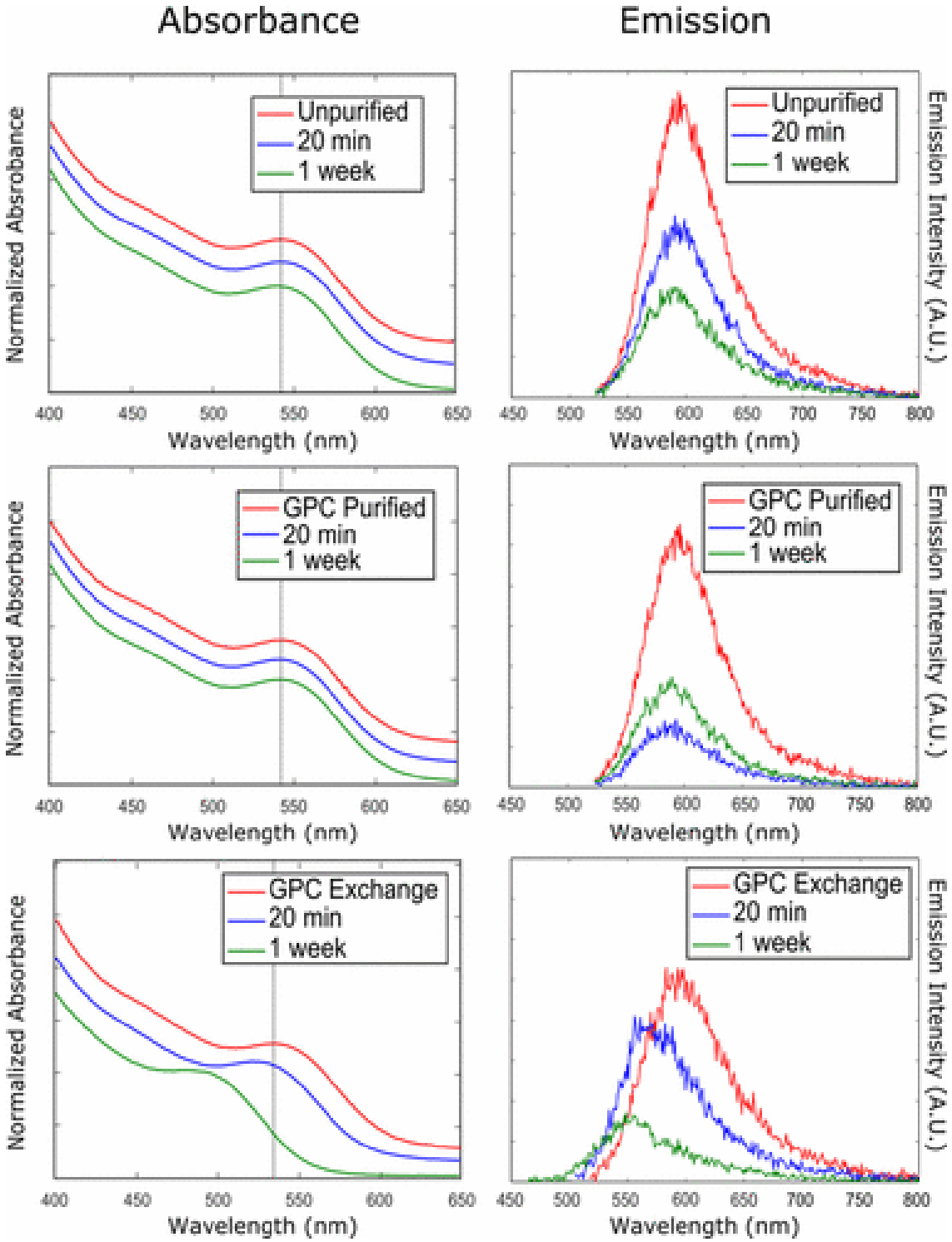

Figure 3.17 Normalized absorbance (left) and emission (right) of Cd-InP samples upon exposure to air for unpurified (top), GPC-purified (middle), and GPC-exchanged (bottom) samples. Absorbance spectra are vertically offset for clarity.

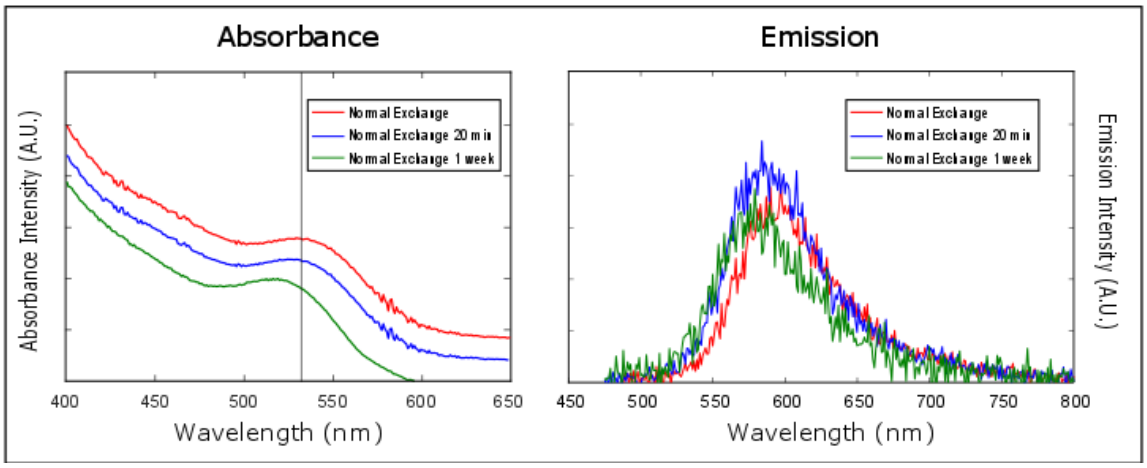

Figure 3.18 Air stability of Cd-InP QD samples undergoing “normal” ligand exchange procedure with HPA showing small change in the absorbance (Left) and emission (Right) after 1 week of air exposure

Chapter 4

Size Dependent PbS QD Surface Chemistry Investigated via Gel Permeation Chromatography

4.1 Introduction

Lead sulfide quantum dots (QDs) have undergone extensive research as their band gap energy and large Bohr radius has made them favorable targets for a variety of optoelectronic applications ranging from photovoltaics to IR sensors.[40–42] Additionally, synthetic methods have been discovered to form PbS QDs with low dispersity in radius over wide a range of sizes.[43–46] Typically, in order to achieve size control, good size distribution, and colloidal stability, long-chain, primarily aliphatic ligands are used during the synthesis. These ligands, while necessary for synthesis, are often exchanged with short chain molecules that increase charge transport in films. In order to optimize these ligand exchange reactions to reduce unused excess of new ligand, knowledge of what the as-synthesized ligand layer is, as well as the quantity of ligands present after synthesis is beneficial. While there have been studies conducted on ligand density on PbS quantum dots, the main purification method employed in these studies is precipitation and redissolution.[47–50] Although this is the most common purification method for semiconductor nanocrystals, it has been demonstrated previously that it can be detrimental to the particles due to changes in solvent environment.[51] As a size-based separation process, gel permeation chromatography (GPC) is an alternative approach to

isolating QDs while maintaining the solvent environment.[23,52] GPC purification of PbS QDs before and after ligand exchange has been reported recently by our group and others,[53,54] but the quantification of the ligand layer was not investigated.[53] Herein we describe the use of GPC to purify oleate-capped PbS QDs of a range of sizes and calculate the ligand density as a function of size. We find that GPC purification of PbS QDs leads to repeatable ligand layers and stable QD solutions.

4.2 Results and Discussion

We synthesized PbS QDs using methods initially described by Hines et al., and more recently detailed by Zhang et al. for accessing a range of QD sizes.[43,44] The measured absorbance spectra (Figure 4.1), in combination with sizing curves published by Moreels et al. were used to calculate the size and concentration of the PbS QDs.[55] The QD sizes used in this study ranged from 2.7-6.1 nm diameter. After synthesis, an initial solvent change from 1-octadecene (ODE) to toluene was effected by one cycle of precipitation and redissolution. The QDs were then purified using gel permeation chromatography (GPC) in toluene mobile phase with a polystyrene gel as the stationary phase. As shown in Figure 4.2, removal of residual ODE and unbound oleate ligands can be observed clearly in ^{1}H NMR spectra of samples before and after the GPC purification step (Figure 4.2). This result, which is achieved with no apparent changes in the electronic absorbance spectra (Figure 4.3), confirms the validity of GPC purification as a method to purify PbS QDs. We note that loading PbS QDs onto the column in pure ODE solvent is unsatisfactory because of its high viscosity and because it is not as good a solvent for the polystyrene gel; purification of PbS QDs without any precipitation and redissolution step can be achieved by dilution of the as-synthesized stock solution in

toluene prior to loading, or by removing a majority of the ODE under high vacuum. Here, we used one cycle of PR to bring the QDs into toluene prior to GPC, in order to increase the amount of QDs that could be purified in a single run of the column. As can be seen in Figure 4.2A, ODE and excess oleate species remain present after the initial PR, and indeed multiple PR cycles are typically required to prepare PbS QDs for optoelectronic applications.[49,56] These additional cycles can be eliminated through the use of GPC.

To determine ligand populations in PbS QD samples, ferrocene (Fc) was employed as an internal standard in the ^{1}H NMR. The total concentration of oleate species [OA] was calculated from the relative strength of the olefin proton resonance:

$$[OA] = [Fc] \times \frac{10}{\int Fc} \times \frac{\int Olefin}{2}$$

By dividing [OA] by the concentration of QDs as determined from the absorbance, a ratio of oleate:QD could be obtained. For comparison among QD samples of varying radius, the oleate ligand population can be expressed as a density per unit area using an assumption of pseudospherical particles. Our results, compiled from three independent GPC purification runs in each case, are listed in Table 4.1 for the size range tested. The ligand density decreases with increasing QD size over the size ranges tested. This can be understood partly as a relaxed steric constraint in small particles due to the greater volume available per ligand on surfaces of high convex curvature. However, charge balance must also be considered as oleate ligands on PbS QDs are generally compensated by excess lead ions on the surface compared to the bulk PbS stoichiometry. Choi et al. showed that PbS QDs undergo a sterically driven shape transition that changes the shape of the particle from octahedral to cuboctahedral as the diameter increases.[57] In particular, at sizes less than 4 nm in diameter the QD is primarily composed of Pb rich (111) facets,

but as the size increases neutral (100) facets begin to appear. It is this decrease of the Pb rich (111) facets to which we attribute the observed decrease in ligand density.

We note that Beygi et al. examined ligand populations on oleate-capped PbS QDs isolated by PR, and compared the ligand weight percentage determined by elemental analysis to predictions based on octahedral and cuboctahedral atomistic models in which Pb-saturated (111) facets were coordinated by oleate. For comparison, we can estimate of the ligand weight percentage in our samples, considering the mass of a PbS sphere of the size noted and the ligand equivalency per QD from NMR. In a representative sample, the ligand weight percentage obtained this way closely matched the mass loss on heating in thermogravimetric analysis (Figure 4.4). These weight percentages are listed in Table 4.1 and agreed quite well with Beygi et al.'s results for the two smaller sizes. The NMR ligand ratios for the two smaller sizes in Table 4.1 are also in close agreement with NMR-derived ratios reported by Kessler and Dempsey in a recent report on ligand displacement in PbS QDs.[50] However, at the largest size (which was not explored in either of the previous studies), we observe a lower ligand ratio than predicted by Beygi's analysis. We note that the Pb atom density on a fully Pb-rich (111) surface is 6.55 nm^{-2}, which exceeds the density at which oleate ligands can pack on a planar surface.[57] This suggests either diminished (111) facet coverage, or incompletely Pb-polar (111) facets, at the 6 nm size.

While the NMR result in Figure 4.2 is typical for smaller PbS QDs, GPC purification of the largest size QDs (6.1 nm) revealed interesting ligand behavior observable in the ^{1}H NMR (Figure 4.5). After GPC purification, two olefin populations are observed by ^{1}H NMR. Frequently, ligand binding to a nanocrystal is associated with

broadening of NMR peaks, primarily due to slower rotational diffusion of the bound ligand compared to the free ligand. Therefore, it is possible to differentiate bound ligand from free ligand in the NMR. Previously, our group has demonstrated that GPC purification reliably removes small molecules such as excess precursor and weakly associated ligands for other metal chalcogenide and pnictide nanocrystals.[22,23,58] In small PbS QDs, this is also the case, however, in the case of the largest PbS QD samples, a population of free ligands remains even after multiple cycles of GPC purification (Figure 4.6). Diffusion ordered spectroscopy (DOSY) was used to probe the two ligand populations and in particular, to evaluate whether the remaining "unbound" feature, whose chemical shift and peak shape are comparable to free $Pb(OA)_2$ and oleic acid in the same solvent, could represent a population non-covalently bound (physisorbed) to the QDs. In fact, as can be seen in Figure 4.7, the two olefin peaks in the purified QD sample have distinctly diffusion coefficients. The species responsible for the narrower olefin peak diffuses much more rapidly, indicating a smaller effective hydrodynamic diameter characteristic of a freely diffusing species, rather than a physisorbed layer. However, the diffusion coefficient is slower than that of free oleic acid (Figure 4.7) and is closer to that of $Pb(OA)_2$ (Figure 4.7). Based on this and results for more strictly aprotic preparations described below, we assign the narrow peak to free $Pb(OA)_2$. Work from Kessler et al. looked at the reactive displacement of $Pb(OA)_2$ from the surface of PbS utilizing L-type assisted Z-type ligand displacement with tetramethylethylenediamine (TMEDA).[50] They find that not only does reactive displacement with TMEDA allude to faceting differences in differing sizes of PbS QDs, the displaced TMEDA-$Pb(OA)_2$ adduct is in dynamic exchange with $Pb(OA)_2$ at the surface. Alluding to the lability of bound $Pb(OA)_2$, which

we also observe in our largest sized PbS QDs. If, after purification, a certain amount of $Pb(OA)_2$ dissociates from the surface of the particle, this might alter the effective particle size for quantum confinement. However, the absorbance spectra before and after purification show no shift in the 1s absorbance peak (Figure 4.3). Variable temperature (VT) NMR was used to probe this "free" population further (Figure 4.8). The temperature range of −20-40 °C was used and over that range integration of the two peaks shows a shift toward the free population: as the percentage of free ligand increases from 51% to 57%. This change is reversible, as cooling back to room temperature reverts the free ligand population to the initial 56%. Furthermore, there were no apparent changes in the absorbance spectra (Figure 4.9) to indicate any net changes to the particles after the thermal cycling in the VT-NMR. Based on the DOSY result showing a small hydrodynamic radius for the sharp NMR signal, we interpret the result as a slow equilibration between strongly-bound $Pb(OA)_2$ equivalents and freely diffusing $Pb(OA)_2$ in toluene solution. From the VT NMR data we can calculate a standard enthalpy change ΔH from a Van't Hoff plot of $\ln(K)$ versus $1/T$ where K is the equilibrium constant describing dissociation of $Pb(OA)_2$ from those sites that remain occupied at the conclusion of GPC purification. In this interpretation, a filled site (A) equilibrates to vacant site (B) and free ligand (C): A→B+C. Therefore, the simple equilibrium constant can be written as $K=([B][C])/[A]$. Suppose initially $[A]=[A]_o$; $[B]=[C]=0$ where $A_o=N[QD]$ and N is the total number of initially occupied sites per QD. We introduce an extent of dissociation α such that at equilibrium, $[A]=[A]_o(1-\alpha)$, $[B]=[A]_o\alpha$, and $[C]=[A]_o\alpha$ so substituting into K:

$$K=\frac{[A]_o^2\alpha^2}{[A]_o(1-\alpha)}=[A]_o\frac{\alpha^2}{1-\alpha}$$

From integration of the two oleate peaks, the ratio *r* of vacant site (B) to filled site (A) may be expressed as r=[B]/[A]=[C]/[A]= α/(1− α). Solving for α we obtain the following expression:

$$\alpha = \frac{r}{1+r}$$

If we then substitute α into *K* we find:

$$K = [\mathrm{A}]_o \frac{r^2}{1+r}$$

Figure 4.10 shows a plot of $\ln(r^2/(1+r))$ versus $1/T$. An approximately linear dependence is indeed observed, and using the above expression for *K* and the Van't Hoff equation we can calculate ΔH for the reaction, which we find to be ΔH=3.7±0.6 kJ/mol.

We note that a dynamic equilibrium between free and bound ligand species has been reported previously for oleate-capped PbS QDs. though it has not been studied in detail as a function of size. In particular, it was shown that in a Hines synthesis, in which the $Pb(OA)_2$ precursor is formed by decomposition of PbO with oleic acid, the water evolved in this step is not completely removed and the precursor exists as a dimer of lead carboxylate hydrate. It has been proposed that this hydrate leads to a combination of hydroxide and oleate passivation on the surface of the PbS.[59,60] This ligand passivation in combination with excess precursors in solution has in turn been proposed as the basis for the observed dynamic ligand passivation in PbS QDs made from the Hines prep.[47] To investigate the possible influence of water on the ligand passivation, we chose to prepare PbS QDs using strictly anhydrous $Pb(OA)_2$ based off of work from Hendricks et al.[61] Using this anhydrous $Pb(OA)_2$ prepared from trifluoroacetic acid anhydride to synthesize PbS quantum dots, we still find that two oleate species are observed after GPC purification for QDs of larger radius (Figure 4.11). Therefore, it is unlikely that the

observed dynamic oleate passivation is a consequence of hydroxide termination at the surface.

During the synthesis of the anhydrous PbS QDs, we observed that under similar reaction conditions, the resulting nanocrystals were consistently smaller in size compared to those using the Hines synthetic method (Figure 4.12). Specifically, as described in detail by Zhang et al., the temperature and precursor concentrations in the Hines method can be varied to control the size of the QD product.[44] We found that for various representative sets of conditions, the "dry" prep produced smaller particles, with larger effective bandgaps, than did the normal prep. This changed occurred without any significant difference in the overall synthetic yield for PbS formula units in the reactions as determined by absorbance. Only by further increasing the concentration of $Pb(OA)_2$ were we able to make the larger-diameter "dry" sample shown in Figure 4.12 and used in the dynamic equilibrium comparison described above. Theoretical work from Stevenson et al. highlighted the importance that water played in the reaction mechanism of PbS in a Hines prep.[60] Their calculations show that in a Hines prep, $Pb(OA)_2$ is in the form of a dimer stabilized by hydrogen bonds with water. This dimer is the precursor that then reacts with $(TMS)_2S$ to form PbS monomers, the precursor to PbS QD nucleation. It has been shown for a variety of nanocrystal systems that precursor reactivity regulates size and concentration of the resultant nanocrystals. Increasing the precursor reactivity leads to an increased monomer supply that leads to a higher concentration of smaller nanocrystals. Therefore, the different observed QD sizes can be explained by the increased reactivity of the $Pb(OA)_2$ in the absence of water-assisted dimerization as is the case in a typical Hines prep. We note that while Hendricks et al. implemented dry

$Pb(OA)_2$ as a precursor for PbS QDs in combination with substituted thiourea sulfur sources,[61] the influence of adventitious water on size in the Hines prep has not been described previously.

We have shown here that GPC purification in toluene provides a highly repeatable route to separation of PbS QDs from small molecule impurities. For smaller QDs, less than about 4 nm diameter, GPC conveniently yields QDs that are stable with low free ligand concentration, such that ligand ratios and densities can be described precisely. For larger QDs, the use of GPC purification has revealed that the ligand layer of the largest sized nanocrystals exists in a dynamic equilibrium with the surface of the nanocrystal: though the samples are colloidally stable, a substantial concentration of free $Pb(OA)_2$ exists at equilibrium. This equilibrium is independent of potential adventitious water as it is observed in QDs synthesized from anhydrous precursors. Furthermore, the anhydrous synthesis reiterates recent findings as to the PbS QD reaction mechanism where removal of water destabilizes the hydrogen bonded lead oleate dimer, creating a more reactive species, and consequently rapid nucleation with limited growth. Regardless of synthetic method, GPC purification results in stable PbS QD solutions that can be utilized to make devices, as we have recently demonstrated in the formation of photovoltaic junctions between PbS QDs and wide-bandgap silicon carbide substrates.[53]

4.3 Materials and Methods

All materials were used as received without further purification. Lead (II) oxide (PbO, 99.9%), oleic acid (OAH, 90%), acetonitrile (anhydrous, 99.8%), trifluoroacetic acid (99%), trifluoroacetic anhydride (99+%), and triethylamine (99%) were purchased from Alfa Aesar. 1-octadecene (ODE, 90%), bistrimethylsilylsulfide ($(TMS)_2S$, 95%),

and ferrocene (98%) were purchased from Acros Organics. Toluene and Isopropanol (certified ACS) were purchased from Fisher Chemical. Toluene d-8 was purchased from Cambridge Isotope Laboratories. *n*-Octane was purchased from EMD Millipore. Biobeads S-X1 medium (column stationary phase, 14000 MWCO) was purchased from Bio-Rad.

Quantum dots were synthesized using the method described by Luther et al..[43] In brief, PbO, OAH, and ODE were combined in a 50 mL three-neck round-bottom flask and heated *in vacuo* to 100 °C. After switching to N_2 atmosphere, a solution of $(TMS)_2S$ in ODE was injected at 95 °C and was allowed to cool to room temperature. The crude synthesis solution was then collected, acetone (methyl acetate for anhydrous dots) was used to precipitate the QDs. After centrifugation at 5000 rpm for 5 minutes the supernatant was discarded, and the precipitate was dissolved in neat toluene. The solutions were stored in toluene until further analysis. Anhydrous lead oleate ($Pb(OA)_2$) was synthesized using modified procedure from Hendricks et al.[61] In brief, lead trifluoroacetate was synthesized using lead (II) oxide, trifluoroacetic acid, and trifluoroacetic anhydride in acetonitrile solvent. Separately, oleic acid and triethylamine were combined in isopropanol solvent. The addition of lead trifluoroacetate to the oleic acid solution formed a white precipitate. The precipitate was isolated using vacuum filtration, washed with methanol, dried using a Schlenk line, and transferred into a nitrogen glovebox.

GPC purification of QDs was conducted as described previously, using a bed height of approximately 140 mm. Using a toluene eluent, the elution time for the QDs was 10±1 minutes.

Absorbance measurements were recorded using a Cary 5000 UV-Vis-NIR spectrometer. For these measurements, aliquots of PbS QDs were diluted into *n*-octane. GPC purification was performed on ~100 nmol quantities of QDs. The collected eluent was then pumped dry on a Schlenk line and dissolved to ca. 100 μM in d-8 toluene with ferrocene as an internal standard. ^{1}H NMR was performed on a Bruker Avance III 400 MHz using 32 scans with a 30 second T_1 delay, except for variable temperature (VT) NMR recorded using a Bruker Avance III 500 MHz spectrometer.

4.4 Tables and figures

Table 4.1 Ligand population and density for PbS QDs of varying sizes

1s Peak (nm)	Diameter (nm)	OA/Dots	OA/nm^2	Ligand wt%
925	2.77	111±1	4.63± 0.06	3.80E+01
1142	3.38	153±1	4.23 ± 0.08	3.18E+01
1584	6.12	494±48	4.20 ± 0.41	2.02E+01

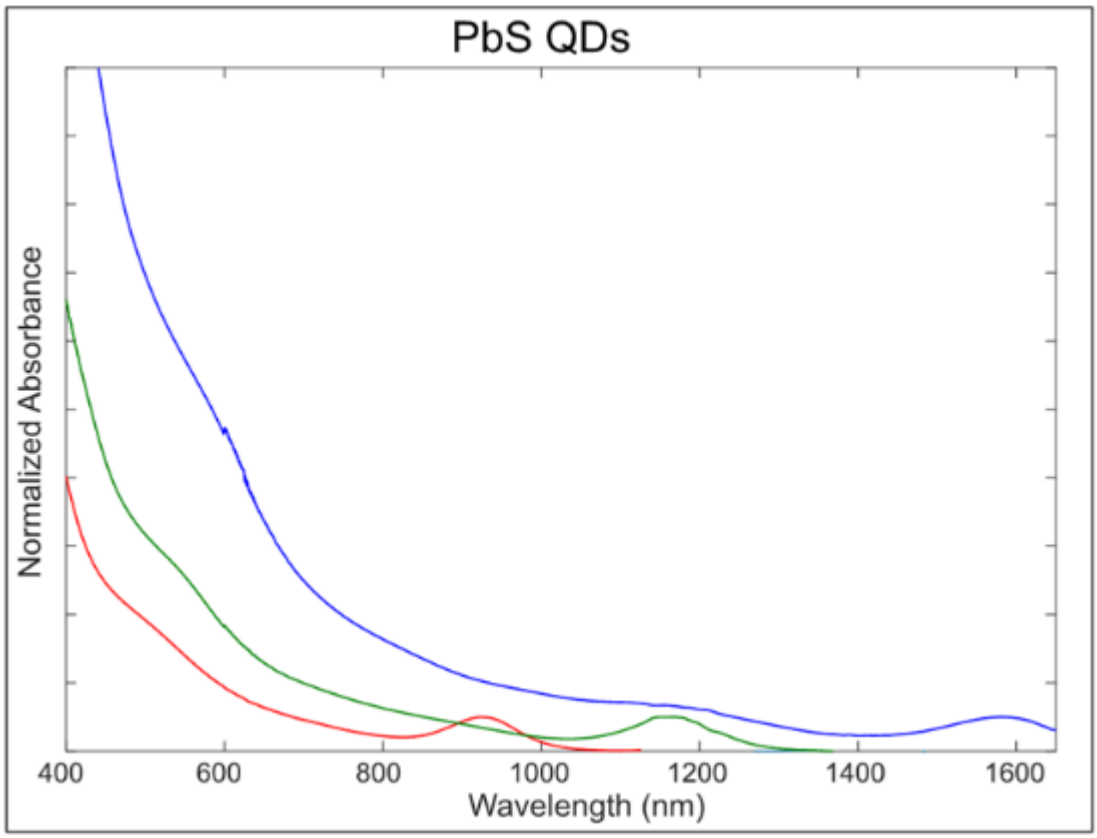

Figure 4.1 Absorbance spectra of PbS QDs normalized to 1s peak intensity

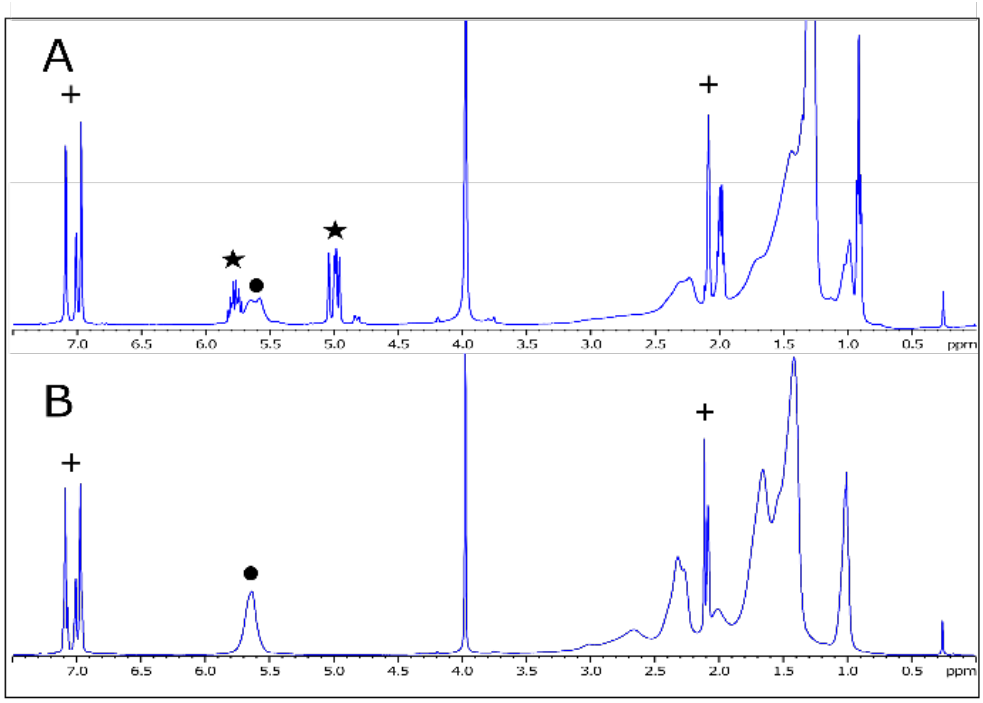

Figure 4.2 ^{1}HNMR of PbS QDs before (A) and after (B) GPC purification. Peaks from growth solvent (★) are removed after purification leaving bound oleate ligands(●)

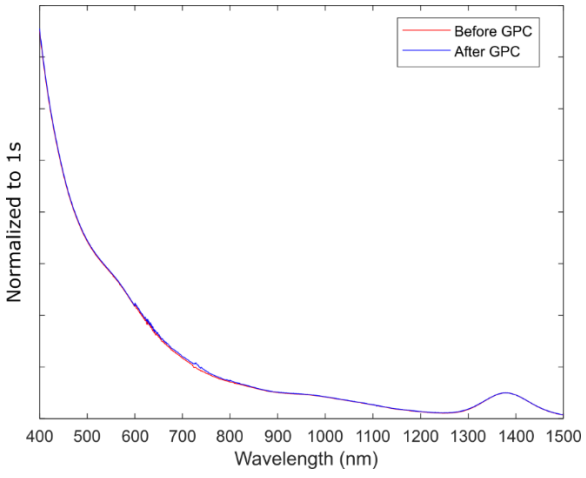

Figure 4.3 Absorbance spectra of PbS QDs before and after GPC purification

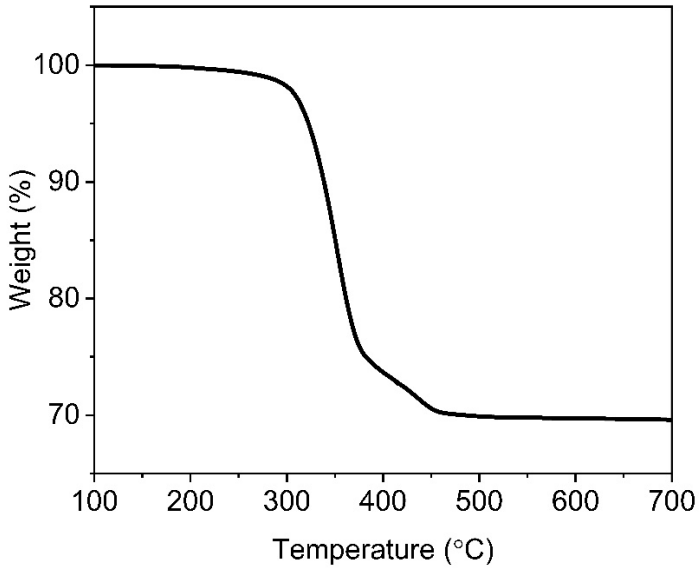

Figure 4.4 Representative thermogravimetric analysis of PbS QDs used to determine ligand weight percentage

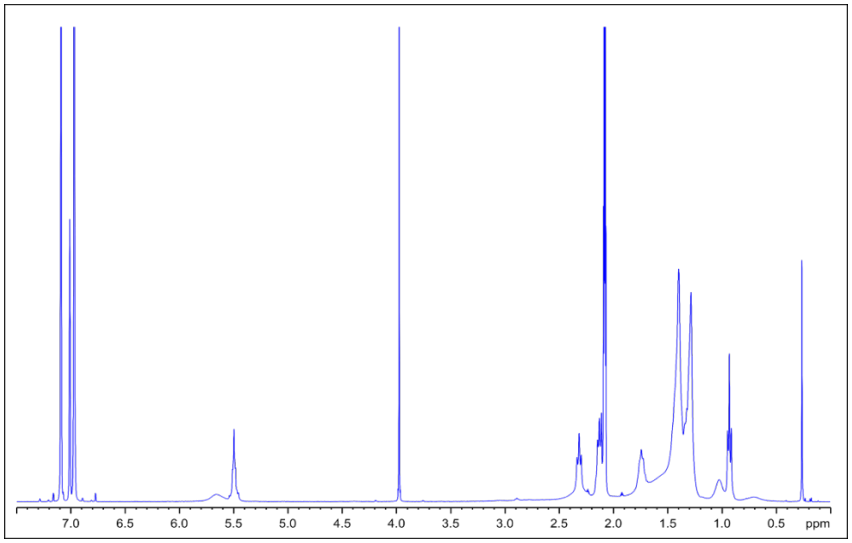

Figure 4.5 ^{1}HNMR of large PbS QDs after purification showing two oleate species

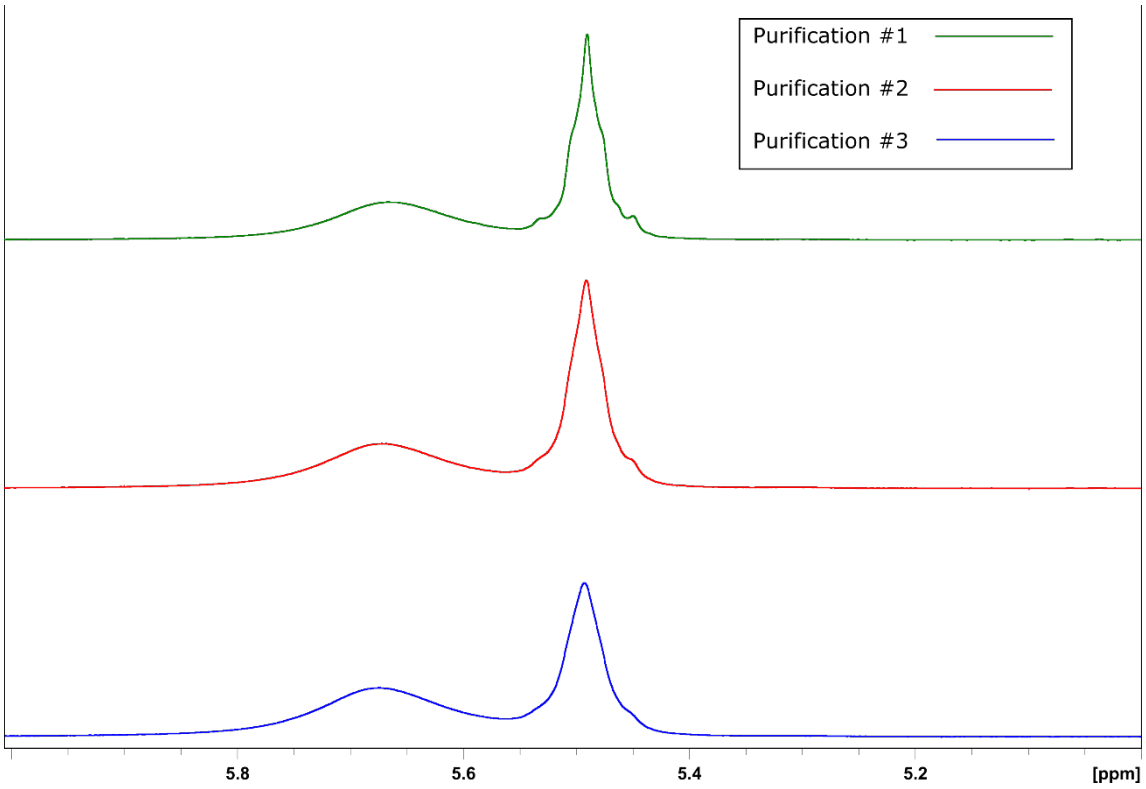

Figure 4.6 [1] HNMR of olefin region for large PbS QDs after multiple purification cycles

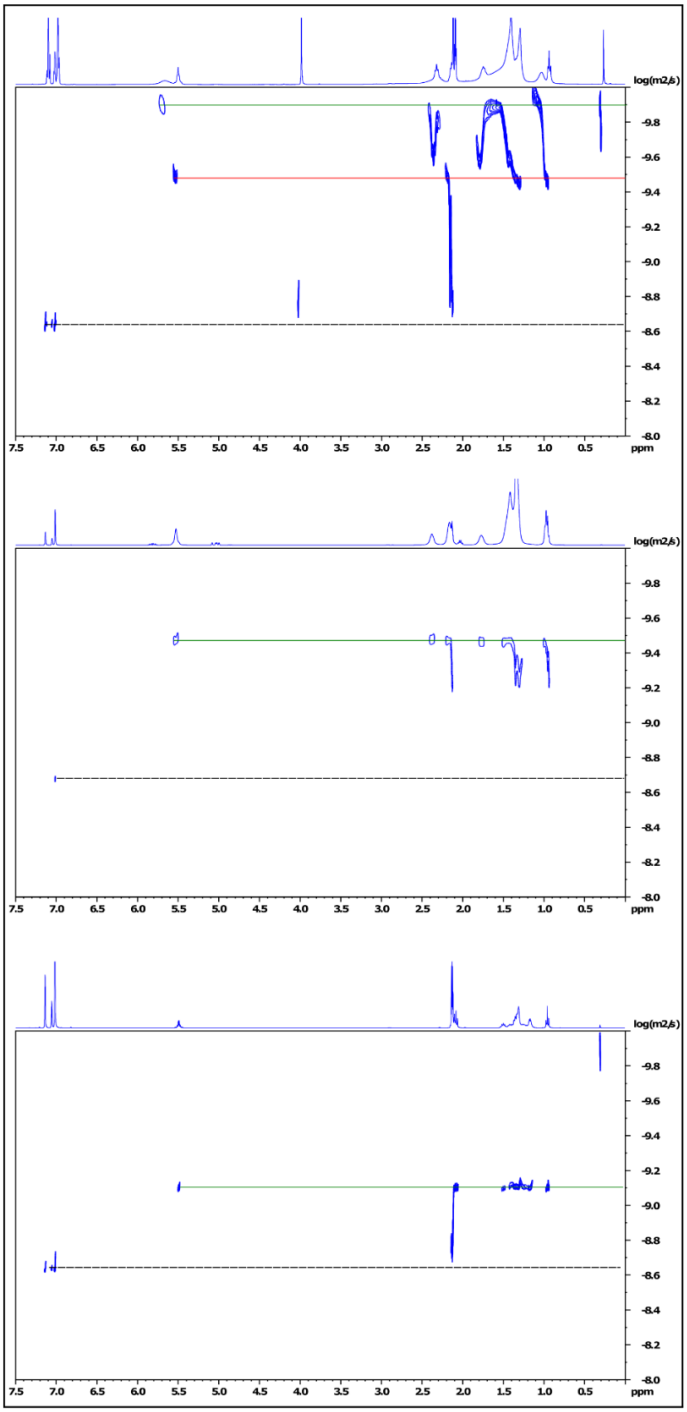

Figure 4.7 Diffusion ordered NMR spectroscopy of PbS QDs (Top), independently prepared $Pb(OA)_2$ (Middle) and oleic acid (Bottom) recorded in toluene.

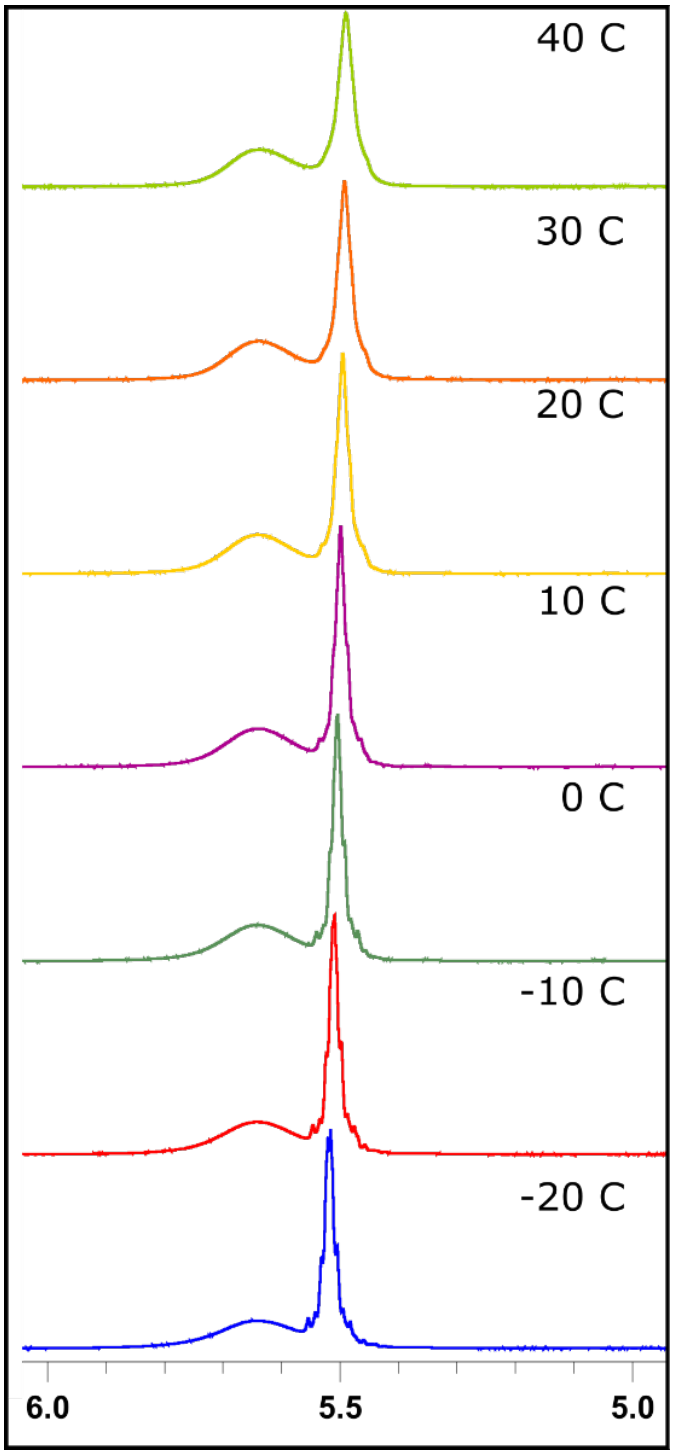

Figure 4.8 Variable temperature ^{1}HNMR of large PbS QDs

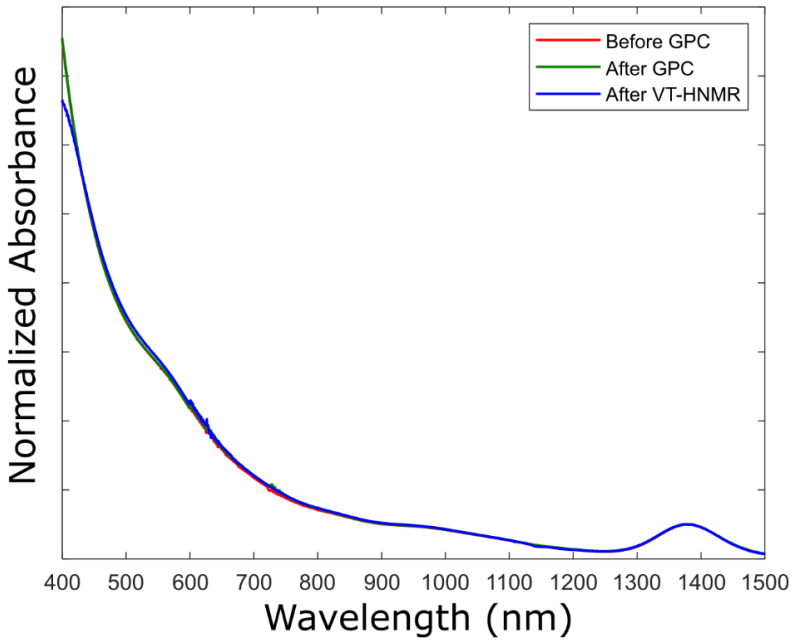

Figure 4.9 Absorbance spectra of PbS QDs before GPC, after GPC, and after VT-HNMR

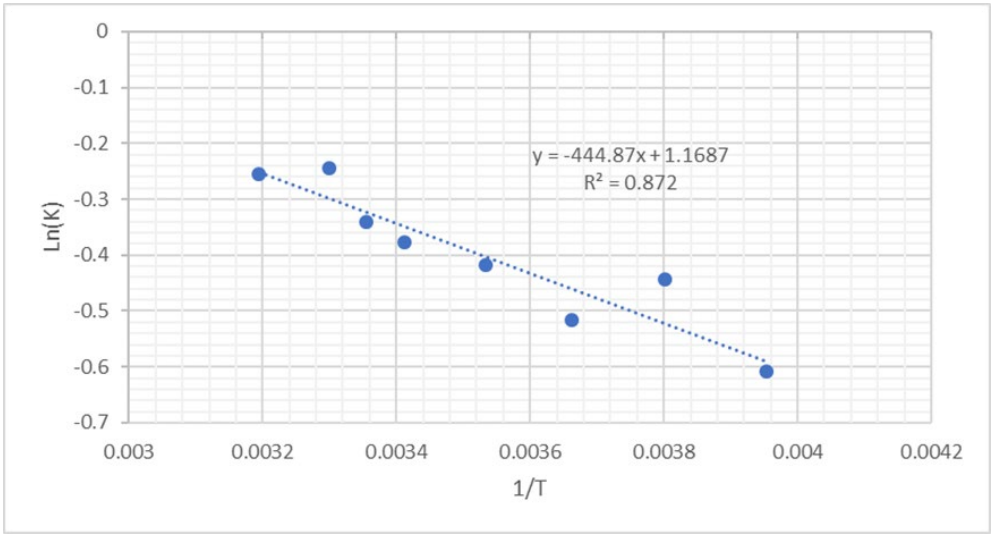

Figure 4.10 Van't Hoff plot for VT-HNMR of large PbS

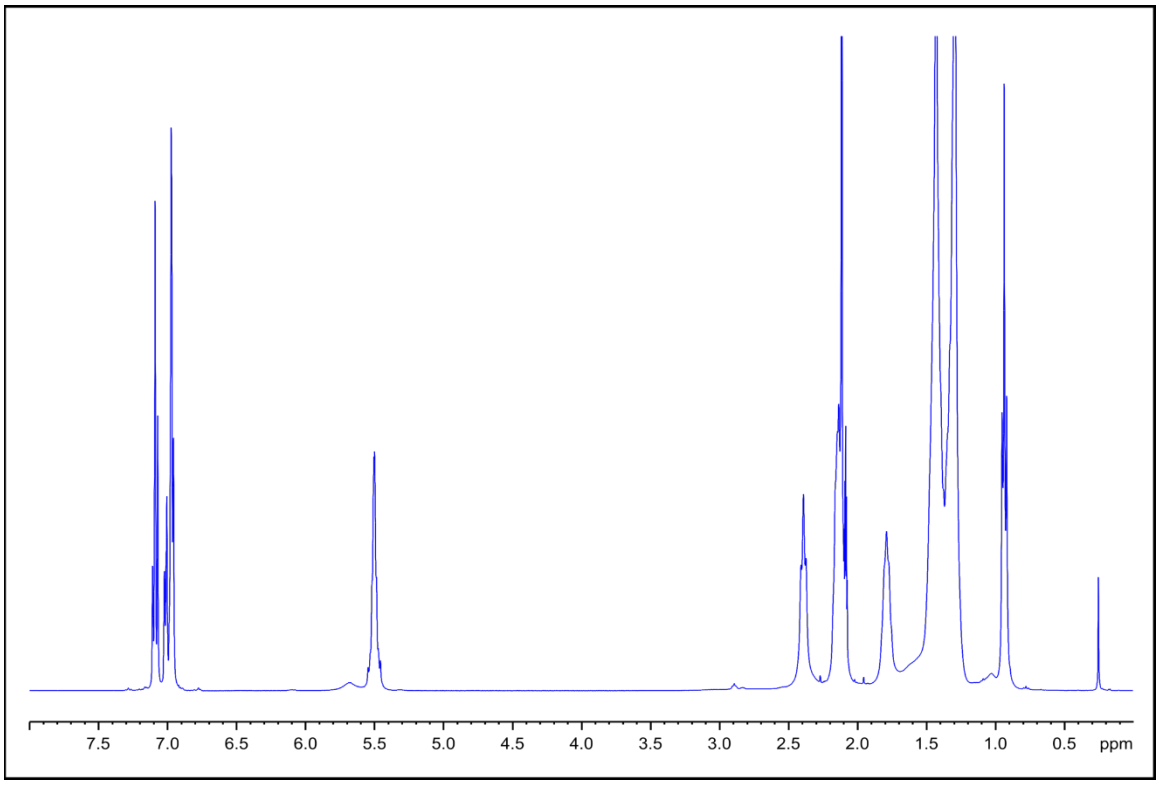

Figure 4.11 ^{1}HNMR of PbS QDs synthesized using anhydrous $Pb(OA)_2$

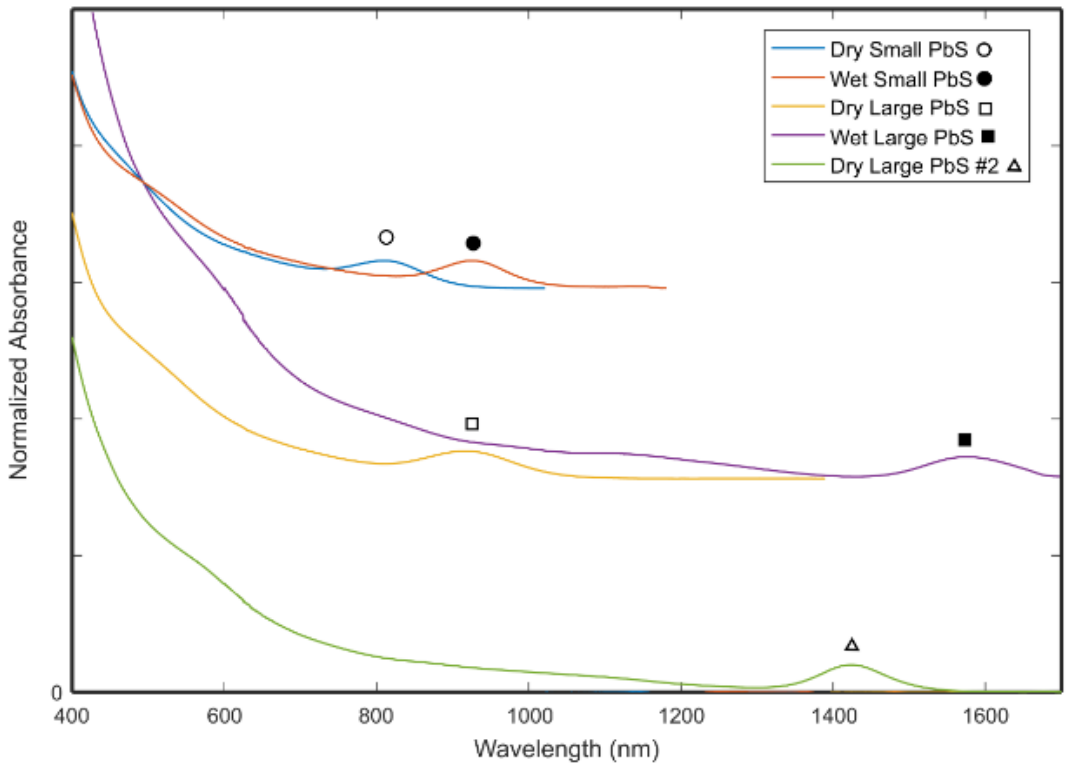

Figure 4.12 Absorbance spectra of PbS made from normal and anhydrous precursors.

References

(1) *Semiconductor Nanocrystal Quantum Dots*; Rogach, A. L., Ed.; Springer Vienna: Vienna, 2008.

(2) Shen, Y.; Tan, R.; Gee, M. Y.; Greytak, A. B. Quantum Yield Regeneration: Influence of Neutral Ligand Binding on Photophysical Properties in Colloidal Core/Shell Quantum Dots. *ACS Nano* **2015**, *9* (3), 3345–3359. https://doi.org/10.1021/acsnano.5b00671.

(3) Giansante, C.; Infante, I.; Fabiano, E.; Grisorio, R.; Suranna, G. P.; Gigli, G. "Darker-than-Black" PbS Quantum Dots: Enhancing Optical Absorption of Colloidal Semiconductor Nanocrystals via Short Conjugated Ligands. *J. Am. Chem. Soc.* **2015**, *137* (5), 1875–1886. https://doi.org/10.1021/ja510739q.

(4) Green, M. L. H. A New Approach to the Formal Classification of Covalent Compounds of the Elements. *J. Organomet. Chem.* **1995**, *500* (1–2), 127–148.

(5) Owen, J. The Coordination Chemistry of Nanocrystal Surfaces. *Science* **2015**, *347* (6222), 615–616. https://doi.org/10.1126/science.1259924.

(6) Murray, C. B.; Norris, D. J.; Bawendi, M. G. Synthesis and Characterization of Nearly Monodisperse CdE (E = Sulfur, Selenium, Tellurium) Semiconductor Nanocrystallites. *J. Am. Chem. Soc.* **1993**, *115* (19), 8706–8715. https://doi.org/10.1021/ja00072a025.

(7) The Heat-Up Synthesis of Colloidal Nanocrystals | Chemistry of Materials https://pubs.acs.org/doi/10.1021/cm5028964 (accessed Mar 1, 2020).

(8) Shen, Y.; Gee, M. Y.; Greytak, A. B. Purification Technologies for Colloidal Nanocrystals. *Chem. Commun.* **2017**, *53* (5), 827–841. https://doi.org/10.1039/C6CC07998A.

(9) Hens, Z.; Martins, J. C. A Solution NMR Toolbox for Characterizing the Surface Chemistry of Colloidal Nanocrystals. *Chem. Mater.* **2013**, *25* (8), 1211–1221. https://doi.org/10.1021/cm303361s.

(10) Tamang, S.; Lincheneau, C.; Hermans, Y.; Jeong, S.; Reiss, P. Chemistry of InP Nanocrystal Syntheses. *Chem. Mater.* **2016**. https://doi.org/10.1021/acs.chemmater.5b05044.

(11) Jasinski, J.; Leppert, V. J.; Lam, S.-T.; Gibson, G. A.; Nauka, K.; Yang, C. C.; Zhou, Z.-L. Rapid Oxidation of InP Nanoparticles in Air. *Solid State Commun.* **2007**, *141* (11), 624–627. https://doi.org/10.1016/j.ssc.2006.12.033.

(12) Xu, S.; Ziegler, J.; Nann, T. Rapid Synthesis of Highly Luminescent InP and InP/ZnS Nanocrystals. *J. Mater. Chem.* **2008**, *18* (23), 2653–2656. https://doi.org/10.1039/B803263G.

(13) Dennis, A. M.; Mangum, B. D.; Piryatinski, A.; Park, Y.-S.; Hannah, D. C.; Casson, J. L.; Williams, D. J.; Schaller, R. D.; Htoon, H.; Hollingsworth, J. A. Suppressed Blinking and Auger Recombination in Near-Infrared Type-II InP/CdS

Nanocrystal Quantum Dots. *Nano Lett.* **2012**, *12* (11), 5545–5551. https://doi.org/10.1021/nl302453x.
(14) Tessier, M. D.; Dupont, D.; De Nolf, K.; De Roo, J.; Hens, Z. Economic and Size-Tunable Synthesis of InP/ZnE (E = S, Se) Colloidal Quantum Dots. *Chem. Mater.* **2015**, *27* (13), 4893–4898. https://doi.org/10.1021/acs.chemmater.5b02138.
(15) Park, J.; Kim, S.; Kim, S.; Yu, S. T.; Lee, B.; Kim, S.-W. Fabrication of Highly Luminescent InP/Cd and InP/CdS Quantum Dots. *J. Lumin.* **2010**, *130* (10), 1825–1828. https://doi.org/10.1016/j.jlumin.2010.04.017.
(16) Li, L.; Reiss, P. One-Pot Synthesis of Highly Luminescent InP/ZnS Nanocrystals without Precursor Injection. *J. Am. Chem. Soc.* **2008**, *130* (35), 11588–11589. https://doi.org/10.1021/ja803687e.
(17) Ryu, E.; Kim, S.; Jang, E.; Jun, S.; Jang, H.; Kim, B.; Kim, S.-W. Step-Wise Synthesis of InP/ZnS Core−Shell Quantum Dots and the Role of Zinc Acetate. *Chem. Mater.* **2009**, *21* (4), 573–575. https://doi.org/10.1021/cm803084p.
(18) Li, J. J.; Wang, Y. A.; Guo, W.; Keay, J. C.; Mishima, T. D.; Johnson, M. B.; Peng, X. Large-Scale Synthesis of Nearly Monodisperse CdSe/CdS Core/Shell Nanocrystals Using Air-Stable Reagents via Successive Ion Layer Adsorption and Reaction. *J. Am. Chem. Soc.* **2003**, *125* (41), 12567–12575. https://doi.org/10.1021/ja0363563.
(19) Tan, R.; Blom, D. A.; Ma, S.; Greytak, A. B. Probing Surface Saturation Conditions in Alternating Layer Growth of CdSe/CdS Core/Shell Quantum Dots. *Chem. Mater.* **2013**, *25* (18), 3724–3736. https://doi.org/10.1021/cm402148s.
(20) Tan, R.; Shen, Y.; Roberts, S. K.; Gee, M. Y.; Blom, D. A.; Greytak, A. B. Reducing Competition by Coordinating Solvent Promotes Morphological Control in Alternating Layer Growth of CdSe/CdS Core/Shell Quantum Dots. *Chem. Mater.* **2015**, *27* (21), 7468–7480. https://doi.org/10.1021/acs.chemmater.5b03588.
(21) Stein, J. L.; Mader, E. A.; Cossairt, B. M. Luminescent InP Quantum Dots with Tunable Emission by Post-Synthetic Modification with Lewis Acids. *J. Phys. Chem. Lett.* **2016**, *7* (7), 1315–1320. https://doi.org/10.1021/acs.jpclett.6b00177.
(22) Shen, Y.; Gee, M. Y.; Tan, R.; Pellechia, P. J.; Greytak, A. B. Purification of Quantum Dots by Gel Permeation Chromatography and the Effect of Excess Ligands on Shell Growth and Ligand Exchange. *Chem. Mater.* **2013**, *25* (14), 2838–2848. https://doi.org/10.1021/cm4012734.
(23) Shen, Y.; Roberge, A.; Tan, R.; Gee, M. Y.; Gary, D. C.; Huang, Y.; Blom, D. A.; Benicewicz, B. C.; Cossairt, B. M.; Greytak, A. B. Gel Permeation Chromatography as a Multifunctional Processor for Nanocrystal Purification and On-Column Ligand Exchange Chemistry. *Chem. Sci.* **2016**, *7* (9), 5671–5679. https://doi.org/10.1039/C6SC01301E.
(24) Talapin, D. V.; Gaponik, N.; Borchert, H.; Rogach, A. L.; Haase, M.; Weller, H. Etching of Colloidal InP Nanocrystals with Fluorides: Photochemical Nature of the Process Resulting in High Photoluminescence Efficiency. *J. Phys. Chem. B* **2002**, *106* (49), 12659–12663. https://doi.org/10.1021/jp026380n.
(25) Xie, L.; Shen, Y.; Franke, D.; Sebastián, V.; Bawendi, M. G.; Jensen, K. F. Characterization of Indium Phosphide Quantum Dot Growth Intermediates Using MALDI-TOF Mass Spectrometry. *J. Am. Chem. Soc.* **2016**, *138* (41), 13469–13472. https://doi.org/10.1021/jacs.6b06468.

(26) Greytak, A. B.; Allen, P. M.; Liu, W.; Zhao, J.; Young, E. R.; Popović, Z.; Walker, B. J.; Nocera, D. G.; Bawendi, M. G. Alternating Layer Addition Approach to CdSe/CdS Core/Shell Quantum Dots with near-Unity Quantum Yield and High on-Time Fractions. *Chem. Sci.* **2012**, *3* (6), 2028–2034. https://doi.org/10.1039/C2SC00561A.
(27) Lawrence, K. N.; Dutta, P.; Nagaraju, M.; Teunis, M. B.; Muhoberac, B. B.; Sardar, R. Dual Role of Electron-Accepting Metal-Carboxylate Ligands: Reversible Expansion of Exciton Delocalization and Passivation of Nonradiative Trap-States in Molecule-like CdSe Nanocrystals. *J. Am. Chem. Soc.* **2016**, *138* (39), 12813–12825. https://doi.org/10.1021/jacs.6b04888.
(28) Gary, D. C.; Petrone, A.; Li, X.; Cossairt, B. M. Investigating the Role of Amine in InP Nanocrystal Synthesis: Destabilizing Cluster Intermediates by Z-Type Ligand Displacement. *Chem. Commun.* **2016**, *53* (1), 161–164. https://doi.org/10.1039/C6CC07952K.
(29) Anderson, N. C.; Hendricks, M. P.; Choi, J. J.; Owen, J. S. Ligand Exchange and the Stoichiometry of Metal Chalcogenide Nanocrystals: Spectroscopic Observation of Facile Metal-Carboxylate Displacement and Binding. *J. Am. Chem. Soc.* **2013**, *135* (49), 18536–18548. https://doi.org/10.1021/ja4086758.
(30) Thuy, U. T. D.; Reiss, P.; Liem, N. Q. Luminescence Properties of In(Zn)P Alloy Core/ZnS Shell Quantum Dots. *Appl. Phys. Lett.* **2010**, *97* (19), 193104. https://doi.org/10.1063/1.3515417.
(31) Siramdas, R.; McLaurin, E. J. InP Nanocrystals with Color-Tunable Luminescence by Microwave-Assisted Ionic-Liquid Etching. *Chem. Mater.* **2017**, *29* (5), 2101–2109. https://doi.org/10.1021/acs.chemmater.6b04457.
(32) Doris, S. E.; Lynch, J. J.; Li, C.; Wills, A. W.; Urban, J. J.; Helms, B. A. Mechanistic Insight into the Formation of Cationic Naked Nanocrystals Generated under Equilibrium Control. *J. Am. Chem. Soc.* **2014**, *136* (44), 15702–15710. https://doi.org/10.1021/ja508675t.
(33) Li, H.; Zanella, M.; Genovese, A.; Povia, M.; Falqui, A.; Giannini, C.; Manna, L. Sequential Cation Exchange in Nanocrystals: Preservation of Crystal Phase and Formation of Metastable Phases. *Nano Lett.* **2011**, *11* (11), 4964–4970. https://doi.org/10.1021/nl202927a.
(34) Marek, H. S.; Serreze, H. B. Diffusion Coefficients and Activation Energies for Zn Diffusion into Undoped and S-doped InP. *Appl. Phys. Lett.* **1987**, *51* (24), 2031–2033. https://doi.org/10.1063/1.98981.
(35) Chakraborty, P.; Jin, Y.; Barrows, C. J.; Dunham, S. T.; Gamelin, D. R. Kinetics of Isovalent (Cd2+) and Aliovalent (In3+) Cation Exchange in Cd1–XMnxSe Nanocrystals. *J. Am. Chem. Soc.* **2016**, *138* (39), 12885–12893. https://doi.org/10.1021/jacs.6b05949.
(36) Gomes, R.; Hassinen, A.; Szczygiel, A.; Zhao, Q.; Vantomme, A.; Martins, J. C.; Hens, Z. Binding of Phosphonic Acids to CdSe Quantum Dots: A Solution NMR Study. *J. Phys. Chem. Lett.* **2011**, *2* (3), 145–152. https://doi.org/10.1021/jz1016729.
(37) Knauf, R. R.; Lennox, J. C.; Dempsey, J. L. Quantifying Ligand Exchange Reactions at CdSe Nanocrystal Surfaces. *Chem. Mater.* **2016**, *28* (13), 4762–4770. https://doi.org/10.1021/acs.chemmater.6b01827.

(38) Cros-Gagneux, A.; Delpech, F.; Nayral, C.; Cornejo, A.; Coppel, Y.; Chaudret, B. Surface Chemistry of InP Quantum Dots: A Comprehensive Study. *J. Am. Chem. Soc.* **2010**, *132* (51), 18147–18157. https://doi.org/10.1021/ja104673y.
(39) Gary, D. C.; Terban, M. W.; Billinge, S. J. L.; Cossairt, B. M. Two-Step Nucleation and Growth of InP Quantum Dots via Magic-Sized Cluster Intermediates. *Chem. Mater.* **2015**, *27* (4), 1432–1441. https://doi.org/10.1021/acs.chemmater.5b00286.
(40) Kang, I.; Wise, F. W. Electronic Structure and Optical Properties of PbS and PbSe Quantum Dots. *JOSA B* **1997**, *14* (7), 1632–1646. https://doi.org/10.1364/JOSAB.14.001632.
(41) Kovalenko, M. V.; Manna, L.; Cabot, A.; Hens, Z.; Talapin, D. V.; Kagan, C. R.; Klimov, V. I.; Rogach, A. L.; Reiss, P.; Milliron, D. J.; Guyot-Sionnnest, P.; Konstantatos, G.; Parak, W. J.; Hyeon, T.; Korgel, B. A.; Murray, C. B.; Heiss, W. Prospects of Nanoscience with Nanocrystals. *ACS Nano* **2015**, *9* (2), 1012–1057. https://doi.org/10.1021/nn506223h.
(42) Sargent, E. H. Colloidal Quantum Dot Solar Cells. *Nat. Photonics* **2012**, *6* (3), 133–135.
(43) Hines, M. a.; Scholes, G. d. Colloidal PbS Nanocrystals with Size-Tunable Near-Infrared Emission: Observation of Post-Synthesis Self-Narrowing of the Particle Size Distribution. *Adv. Mater.* **2003**, *15* (21), 1844–1849. https://doi.org/10.1002/adma.200305395.
(44) Zhang, J.; Crisp, R. W.; Gao, J.; Kroupa, D. M.; Beard, M. C.; Luther, J. M. Synthetic Conditions for High-Accuracy Size Control of PbS Quantum Dots. *J. Phys. Chem. Lett.* **2015**, *6* (10), 1830–1833. https://doi.org/10.1021/acs.jpclett.5b00689.
(45) Moreels, I.; Justo, Y.; De Geyter, B.; Haustraete, K.; Martins, J. C.; Hens, Z. Size-Tunable, Bright, and Stable PbS Quantum Dots: A Surface Chemistry Study. *ACS Nano* **2011**, *5* (3), 2004–2012. https://doi.org/10.1021/nn103050w.
(46) Dong, C.; Liu, S.; Barange, N.; Lee, J.; Pardue, T.; Yi, X.; Yin, S.; So, F. Long-Wavelength Lead Sulfide Quantum Dots Sensing up to 2600 Nm for Short-Wavelength Infrared Photodetectors. *ACS Appl. Mater. Interfaces* **2019**, *11* (47), 44451–44457. https://doi.org/10.1021/acsami.9b16539.
(47) Grisorio, R.; Debellis, D.; Suranna, G. P.; Gigli, G.; Giansante, C. The Dynamic Organic/Inorganic Interface of Colloidal PbS Quantum Dots. *Angew. Chem. Int. Ed.* **2016**, *55* (23), 6628–6633. https://doi.org/10.1002/anie.201511174.
(48) Beygi, H.; Sajjadi, S. A.; Babakhani, A.; Young, J. F.; van Veggel, F. C. J. M. Surface Chemistry of As-Synthesized and Air-Oxidized PbS Quantum Dots. *Appl. Surf. Sci.* **2018**, *457*, 1–10. https://doi.org/10.1016/j.apsusc.2018.06.152.
(49) Weir, M. P.; Toolan, D. T. W.; Kilbride, R. C.; Penfold, N. J. W.; Washington, A. L.; King, S. M.; Xiao, J.; Zhang, Z.; Gray, V.; Dowland, S.; Winkel, J.; Greenham, N. C.; Friend, R. H.; Rao, A.; Ryan, A. J.; Jones, R. A. L. Ligand Shell Structure in Lead Sulfide–Oleic Acid Colloidal Quantum Dots Revealed by Small-Angle Scattering. *J. Phys. Chem. Lett.* **2019**, *10* (16), 4713–4719. https://doi.org/10.1021/acs.jpclett.9b01008.
(50) Kessler, M. L.; Dempsey, J. L. Mapping the Topology of PbS Nanocrystals through Displacement Isotherms of Surface-Bound Metal Oleate Complexes.

Chem. Mater. **2020**, *32* (6), 2561–2571. https://doi.org/10.1021/acs.chemmater.0c00014.
(51) Hassinen, A.; Moreels, I.; De Nolf, K.; Smet, P. F.; Martins, J. C.; Hens, Z. Short-Chain Alcohols Strip X-Type Ligands and Quench the Luminescence of PbSe and CdSe Quantum Dots, Acetonitrile Does Not. *J. Am. Chem. Soc.* **2012**, *134* (51), 20705–20712. https://doi.org/10.1021/ja308861d.
(52) Shen, Y.; Gee, M. Y.; Greytak, A. B. Purification Technologies for Colloidal Nanocrystals. *Chem Commun* **2017**, *53* (5), 827–841. https://doi.org/10.1039/C6CC07998A.
(53) Kelley, M. L.; Letton, J.; Simin, G.; Ahmed, F.; Love-Baker, C. A.; Greytak, A. B.; Chandrashekhar, M. V. S. Photovoltaic and Photoconductive Action Due to PbS Quantum Dots on Graphene/SiC Schottky Diodes from NIR to UV. *ACS Appl. Electron. Mater.* **2020**, *2* (1), 134–139. https://doi.org/10.1021/acsaelm.9b00651.
(54) Kroupa, D. M.; Arias, D. H.; Blackburn, J. L.; Carroll, G. M.; Granger, D. B.; Anthony, J. E.; Beard, M. C.; Johnson, J. C. Control of Energy Flow Dynamics between Tetracene Ligands and PbS Quantum Dots by Size Tuning and Ligand Coverage. *Nano Lett.* **2018**, *18* (2), 865–873. https://doi.org/10.1021/acs.nanolett.7b04144.
(55) Moreels, I.; Lambert, K.; Smeets, D.; De Muynck, D.; Nollet, T.; Martins, J. C.; Vanhaecke, F.; Vantomme, A.; Delerue, C.; Allan, G.; Hens, Z. Size-Dependent Optical Properties of Colloidal PbS Quantum Dots. *ACS Nano* **2009**, *3* (10), 3023–3030. https://doi.org/10.1021/nn900863a.
(56) Carey, G. H.; Abdelhady, A. L.; Ning, Z.; Thon, S. M.; Bakr, O. M.; Sargent, E. H. Colloidal Quantum Dot Solar Cells. *Chem. Rev.* **2015**, *115* (23), 12732–12763. https://doi.org/10.1021/acs.chemrev.5b00063.
(57) Choi, H.; Ko, J.-H.; Kim, Y.-H.; Jeong, S. Steric-Hindrance-Driven Shape Transition in PbS Quantum Dots: Understanding Size-Dependent Stability. *J. Am. Chem. Soc.* **2013**, *135* (14), 5278–5281. https://doi.org/10.1021/ja400948t.
(58) Roberge, A.; Stein, J. L.; Shen, Y.; Cossairt, B. M.; Greytak, A. B. Purification and In Situ Ligand Exchange of Metal-Carboxylate-Treated Fluorescent InP Quantum Dots via Gel Permeation Chromatography. *J. Phys. Chem. Lett.* **2017**, 4055–4060. https://doi.org/10.1021/acs.jpclett.7b01772.
(59) Zherebetskyy, D.; Scheele, M.; Zhang, Y.; Bronstein, N.; Thompson, C.; Britt, D.; Salmeron, M.; Alivisatos, P.; Wang, L.-W. Hydroxylation of the Surface of PbS Nanocrystals Passivated with Oleic Acid. *Science* **2014**, *344* (6190), 1380–1384. https://doi.org/10.1126/science.1252727.
(60) Stevenson, J. M.; Ruttinger, A. W.; Clancy, P. Uncovering the Reaction Mechanism Initiating the Nucleation of Lead Sulfide Quantum Dots in a Hines Synthesis. *J. Mater. Chem. A* **2018**, *6* (20), 9402–9410. https://doi.org/10.1039/C8TA00220G.
(61) Hendricks, M. P.; Campos, M. P.; Cleveland, G. T.; Plante, I. J.-L.; Owen, J. S. A Tunable Library of Substituted Thiourea Precursors to Metal Sulfide Nanocrystals. *Science* **2015**, *348* (6240), 1226–1230. https://doi.org/10.1126/science.aaa2951.